

# On the Sources and Sizes of Error in Predicting the Arrival Time of Interplanetary Coronal Mass Ejections using Global MHD Models

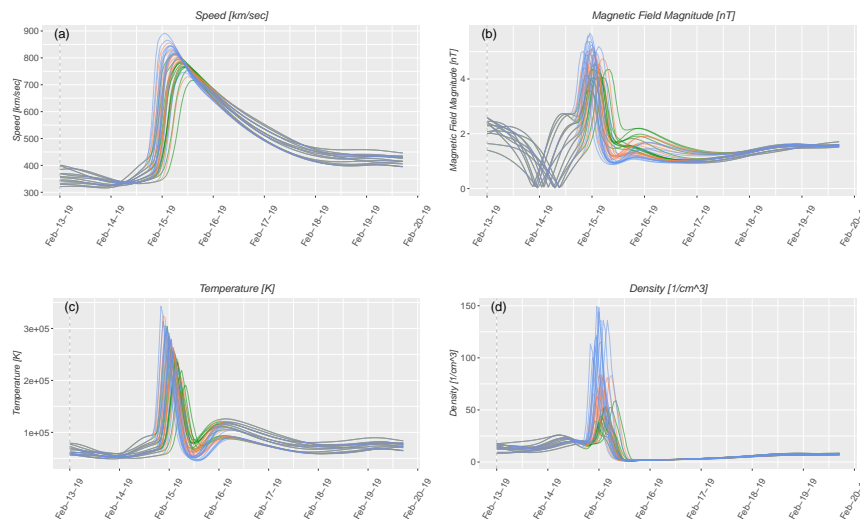
Pete Riley<sup>1</sup> and michal Ben-Nun<sup>1</sup>

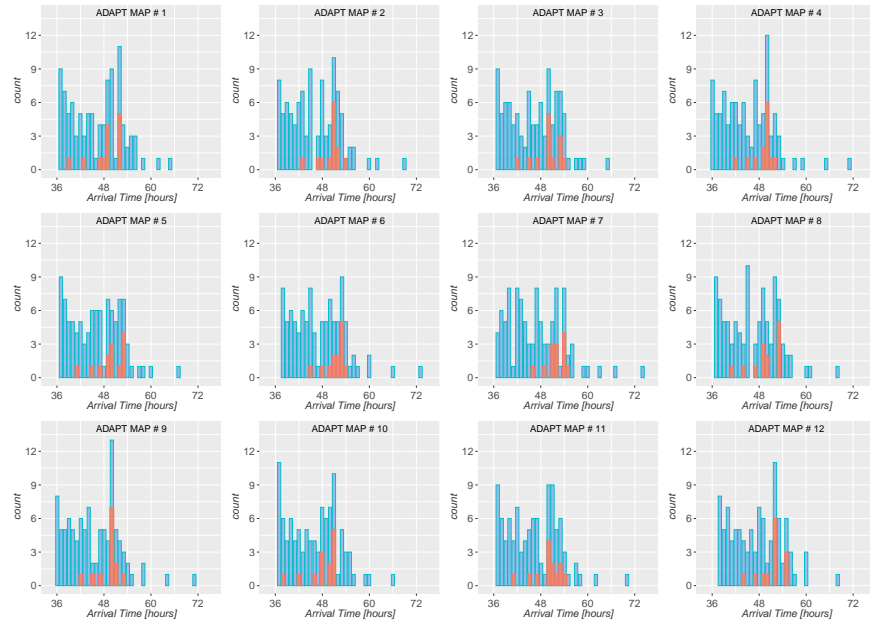
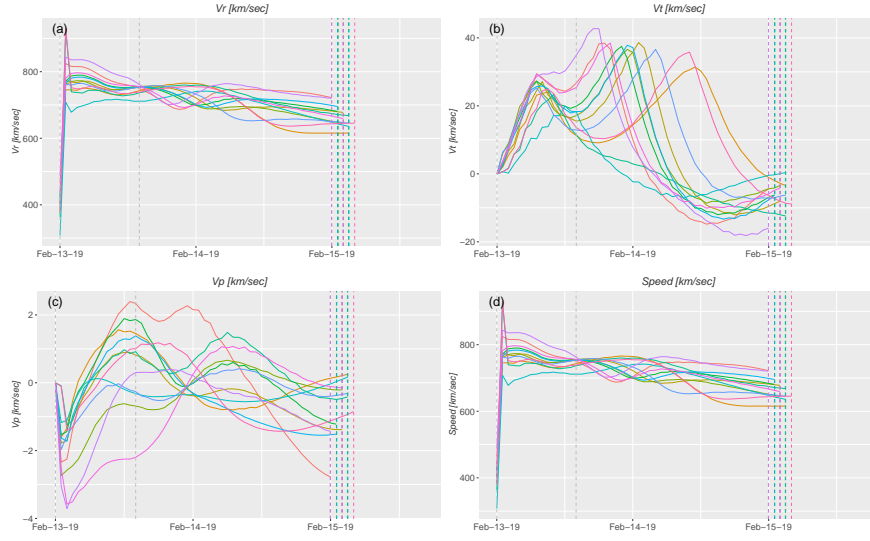
<sup>1</sup>Predictive Science Inc.

November 22, 2022

## Abstract

Accurate predictions of the properties of interplanetary coronal mass ejection (ICME)-driven disturbances are a key objective for space weather forecasts. The ICME's time of arrival (ToA) at Earth is an important parameter and one that is amenable to a variety of modeling approaches. Previous studies suggest that the best models can predict the arrival time to within an absolute error of 10-15 hours. Here, we investigate the main sources of error in predicting a CME's ToA at Earth. These can be broken into two main categories: (1) the initial properties of the ejecta, including its speed, mass, and direction of propagation; and (2) the properties of the ambient solar wind into which it propagates. To estimate the relative contribution to ToA errors, we construct a set of numerical experiments of cone-model CMEs, where we vary the initial speed, mass, and direction at the inner radial boundary. Additionally, we build an ensemble of 12 ambient solar wind solutions using realizations from the ADAPT model. We find that each component in the chain contributes between  $\pm 2.5$  and  $\pm 7$  hours of uncertainty to the estimate of the CME's ToA. Importantly, different realizations of the synoptic produce the largest errors. This suggests that estimates of ToA will continue to be plagued with intrinsic errors of  $\pm 10$  hours until tighter constraints can be found for these boundary conditions. Our results suggest that there are clear benefits to focused investigations aimed at reducing the uncertainties in CME speed, mass, direction, and input boundary magnetic fields.





1       **On the Sources and Sizes of Error in Predicting the Arrival**  
2       **Time of Interplanetary Coronal Mass Ejections using Global**  
3       **MHD Models**

4                               **Pete Riley<sup>1</sup> and Michal Ben-Nun<sup>1</sup>**

5                               <sup>1</sup>Predictive Science Inc., San Diego, USA

6       **Key Points:**

- 7       • Errors in the arrival time of ICMEs derive from a mixture of individual, but identi-  
8       fiable uncertainties in the chain from the Sun to 1 AU  
9       • Different ADAPT realizations produce errors in the arrival time of ICMEs of  $\pm 7$   
10      hours or more.  
11      • Targeted studies aimed at reducing each of the uncertainties would improve the ac-  
12      curacy and precision in the arrival time of ICMEs

**Abstract**

Accurate predictions of the properties of interplanetary coronal mass ejection (ICME)-driven disturbances are a key objective for space weather forecasts. The ICME's time of arrival (ToA) at Earth is an important parameter, and one that is amenable to a variety of modeling approaches. Previous studies suggest that the best models can predict the arrival time to within an absolute error of 10-15 hours. Here, we investigate the main sources of error in predicting a CME's ToA at Earth. These can be broken into two main categories: (1) the initial properties of the ejecta, including its speed, mass, and direction of propagation; and (2) the properties of the ambient solar wind into which it propagates. To estimate the relative contribution to ToA errors, we construct a set of numerical experiments of cone-model CMEs, where we vary the initial speed, mass, and direction at the inner radial boundary. Additionally, we build an ensemble of 12 ambient solar wind solutions using realizations from the ADAPT model. We find that each component in the chain contributes between  $\pm 2.5$  and  $\pm 7$  hours of uncertainty to the estimate of the CME's ToA. Importantly, different realizations of the synoptic produce the largest errors. This suggests that estimates of ToA will continue to be plagued with intrinsic errors of  $\pm 10$  hours until tighter constraints can be found for these boundary conditions. Our results suggest that there are clear benefits to focused investigations aimed at reducing the uncertainties in CME speed, mass, direction, and input boundary magnetic fields.

**Plain Language Summary**

Coronal mass ejections are huge explosions of plasma and magnetic field, which, if they impact the Earth's protective magnetospheric shield, can result in a range of consequences, from increased radiation doses for aircraft passengers to electrical black-outs across large regions. Being able to forecast their properties, as well as when they will arrive at Earth are key objectives for space weather programs. In this study, we have investigated a broad set of uncertainties associated with these predictions, which include the initial specification of the properties of the CME at the Sun as well as the properties of the interplanetary medium into which it propagates. Remarkably, and disappointingly, we find that there are inherent limitations in the accuracy of the forecasts that will not likely be resolved by more sophisticated modeling techniques. Instead, they will require substantial investment in developing more comprehensive datasets to drive the models, which, in turn, will require new space missions. More modest improvements, however, can be made by addressing components in the forecasting system and attempting to reduce (or at least accurately assess) the errors associated with them.

**1 Introduction**

Geomagnetic storms are an essential component of space weather at Earth, and anticipating their onset is one of the major priorities for the National Oceanic and Atmospheric Administration (NOAA) Space Weather Prediction Center (SWPC). The two primary drivers of these storms are fast solar wind streams and coronal mass ejections (CMEs). CMEs are large-scale coronal eruptions that propel plasma and magnetic fields into the solar wind, and are generally responsible for the most severe storms [Gosling *et al.*, 1990]. To provide one- to four-day warning of these storms, NOAA/SWPC operationally implemented the Wang-Sheeley-Argue-ENLIL cone model, or WSA+ENLIL [Pizzo *et al.*, 2011].

Ideally, a comprehensive CME forecasting framework would begin at the Sun, using first-principles models [e.g., Forbes and Lin, 2000], and provide the longest lead-time for predictions. However, in practice, models capable of mimicking the eruption of the CME and its evolution in the corona remain idealised and the subject of fundamental research, not operational forecasting [Török *et al.*, 2018]. Thus, current forecasting models blend elements of empiricism and domain reduction to provide tractable solutions. For example,

63 CMEs are often treated as hydrodynamic “pulses”, usually inserted high in the corona,  
 64 with properties inferred from relevant observations [e.g., *Riley et al.*, 2003; *Odstrcil et al.*,  
 65 2004].

66 The WSA+ENLIL forecasting system is a good example of the general approach  
 67 applied by a number of groups [*Riley et al.*, 2018], and proceeds in the following man-  
 68 ner: Magnetic maps of the solar magnetic field in the photosphere, obtained from ground-  
 69 and/or space-based observatories [*Riley et al.*, 2014], are used to compute potential field  
 70 models of the solar corona. An empirical prescription for the solar wind speed based on  
 71 magnetic field structure, the Wang-Sheeley-Arge (WSA) model [*Arge et al.*, 2003], is used  
 72 to specify boundary conditions for the ENLIL magnetohydrodynamic (MHD) model of the  
 73 solar wind [*Odstrcil et al.*, 2003]. ENLIL is integrated in time until a steady-state back-  
 74 ground solar wind solution is reached beyond 1 AU. This solution is typically updated sev-  
 75 eral times a day, as new magnetograms are made available. When observed, “cone-model”  
 76 CMEs are injected into the flow and tracked out to 1 AU [e.g., *Pizzo et al.*, 2011].

77 Several previous studies have investigated the WSA+ENLIL forecasting system.  
 78 *Pizzo et al.* [2015], for example, explored the effects of launching a range of cone-model  
 79 CMEs into different idealized ambient solar wind states. In particular, they developed  
 80 a set of idealised numerical experiments, propagating a series of CME pulses into (1) a  
 81 uniform (spherically symmetric background); and (2) tilted-dipole stream structure. They  
 82 found relatively predictable patterns in the time of arrival (ToA) of ICMEs as a function  
 83 of the initial properties of the ejecta, and ruled out the possibility of any chaotic behaviour  
 84 that might manifest itself in the forecasts.

85 *Mays et al.* [2015] developed ensemble model results for 35 observed CME events  
 86 occurring between January 2013 and July 2014. For those events that were predicted to  
 87 arrive at earth (17 events), they estimated the MAE error in ToA prediction of 12.3 hours.  
 88 They also estimated correct and false-alarm ratios for these events. They suggested that  
 89 the accuracy of the predicted arrival time was sensitive to the initial distribution of CME  
 90 parameters, and that for their analyses, the spread was probably underestimated.

91 *Riley et al.* [2018] summarized a large number of CME forecasting tools and com-  
 92 pared their forecasting capabilities with one another. They addressed: (1) How well the  
 93 models predicted the arrival time of CME-driven shocks at Earth? (2) What were the er-  
 94 rors associated with these forecasts? (3) Which, if any models performed better? and (4)  
 95 Did any of the models had demonstrate improvements in accuracy over the six-year period  
 96 that they had been in use? They found that, for the best models, CME-shock arrival times  
 97 could be predicted with  $\pm 1$  hour (mean error) or  $\pm 13$  hours (mean absolute error), with a  
 98 precision (standard deviation) of 15 hours. However, they also inferred that there had been  
 99 no measurable improvement in model accuracy during the six-year interval that predictions  
 100 had been made.

101 In this study, we build upon these earlier investigations in several important ways.  
 102 First, we consider the propagation of CME pulses through a set of 12 ADAPT-GONG re-  
 103 alizations of the photospheric magnetic field. These are estimates of the synchronic field  
 104 that are, in principle all likely to be equally valid, or at least consistent with the available  
 105 observations. Second, we consider the propagation of a large number of CME pulses that  
 106 are representative of a fast CME with a distribution in properties that are consistent with  
 107 the likely uncertainties in their measured values. Third, we estimate the contributions to  
 108 the estimated errors in arrival time due to each component (or model parameter) in the  
 109 modeled system.

## 2 Methods

### 2.1 Data

For this study, we use ADAPT-GONG quasi-synchronic magnetograms [Arge *et al.*, 2010]. These are “quasi-” or “pseudo-” synchronic in the sense that only observations from Earth-based solar observatories are used to generate each map at each point in time, and photospheric magnetic flux transport processes are invoked to evolve the magnetic field distribution as it drifts westward and beyond the observation window. Additionally, data assimilation techniques are used to update the modelled flux with new observations. In principle, this can account for both model and observational uncertainties, and, importantly, allows for the generation of multiple realizations at each point in time. For the purposes of computing MHD solutions, we further process the magnetograms by smoothing them, extrapolating mid-latitude data poleward, and removing any monopole components [e.g., Riley *et al.*, 2012].

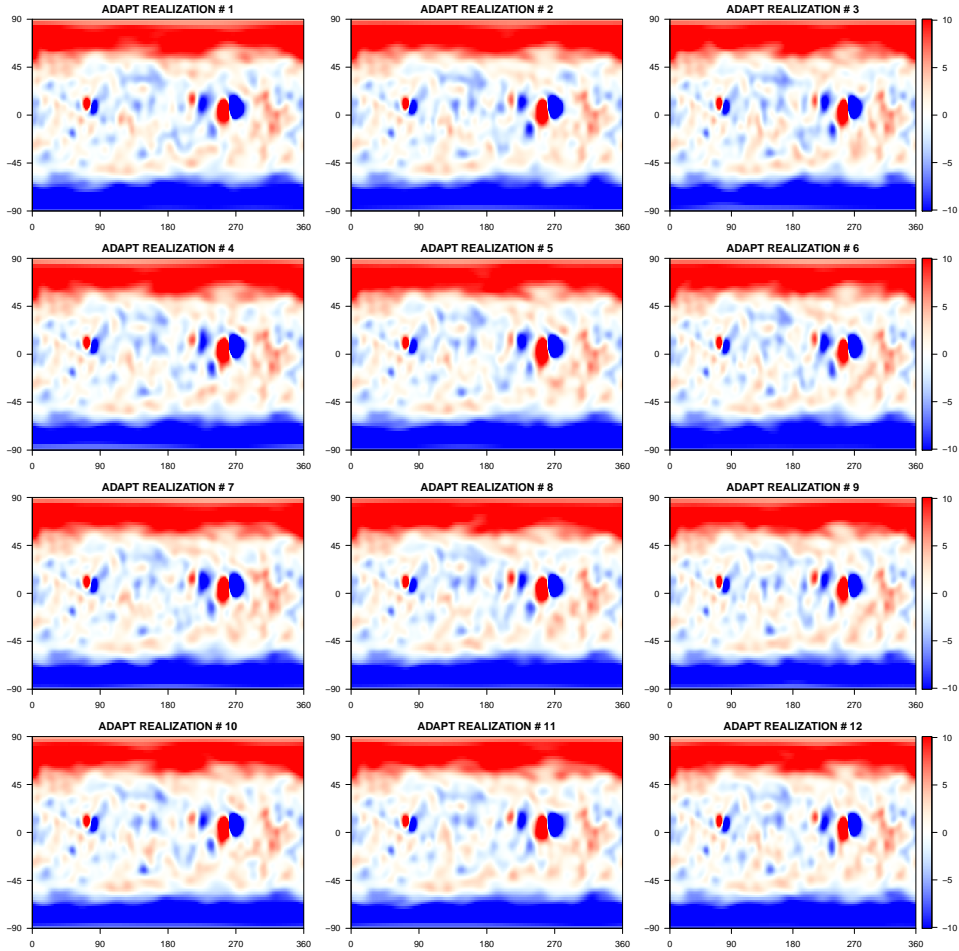
We chose Carrington Rotation (CR) 2207 (09/02/2018 - 09/29/2018) for our analysis since it occurred during a time period that was: (1) relatively stable from one rotation to the next; (2) exhibited a simple solar minimum-like configuration with slow flow emanating from about the equator and large polar coronal holes producing fast, steady solar wind at higher latitudes; and (3) devoid of any significant CME activity. Figure 1 summarizes 12 realizations of ADAPT/GONG synchronic maps corresponding to the midpoint in time of CR 2207.

We note several points. First, overall, the realizations look very similar to one another. The two main clusters of active regions (at  $80^\circ$  and  $240^\circ$ ) appear to be nearly identical, as does the overall structure of the polar regions. It is worth noting, however, that the fields have been visually saturated at  $\pm 10$  G. Second, at smaller scales there are some subtle differences. For example, the structure of the polar regions, as evidenced by contours near  $\pm 10$  G (the boundary between deep red/blue and white), changes from one realization to the next. In particular, the white excursions into the otherwise red/blue polar regions occur at slightly different longitudes from one panel to the next. Third, the shape of the active region (AR) fields, including the orientation of the bipoles, changes modestly from one realization to the next. Additionally, the strength of the AR fields is not the same. For example, consider the negative flux region south of, but between the two major ARs at  $\sim 240^\circ$  longitude. This is much weaker in realization 11 than in realization 12. These are, however, minor differences, and it is not clear based only on these maps what impact, if any, they may have on the evolution of CMEs in the solar wind. Only by simulating an ICME through all solutions can we assess their impact on the ToA of the ICME. It is, however, worth underscoring that these ADAPT realizations are just that: synchronic maps that are all consistent with the available observations. Thus, we cannot – a priori – say that one is better than another, and so they provide a useful way to capture (or, at least, provide a lower limit to) uncertainties due to the ambient boundary conditions.

### 2.2 Models

#### 2.2.1 Ambient Solar Wind

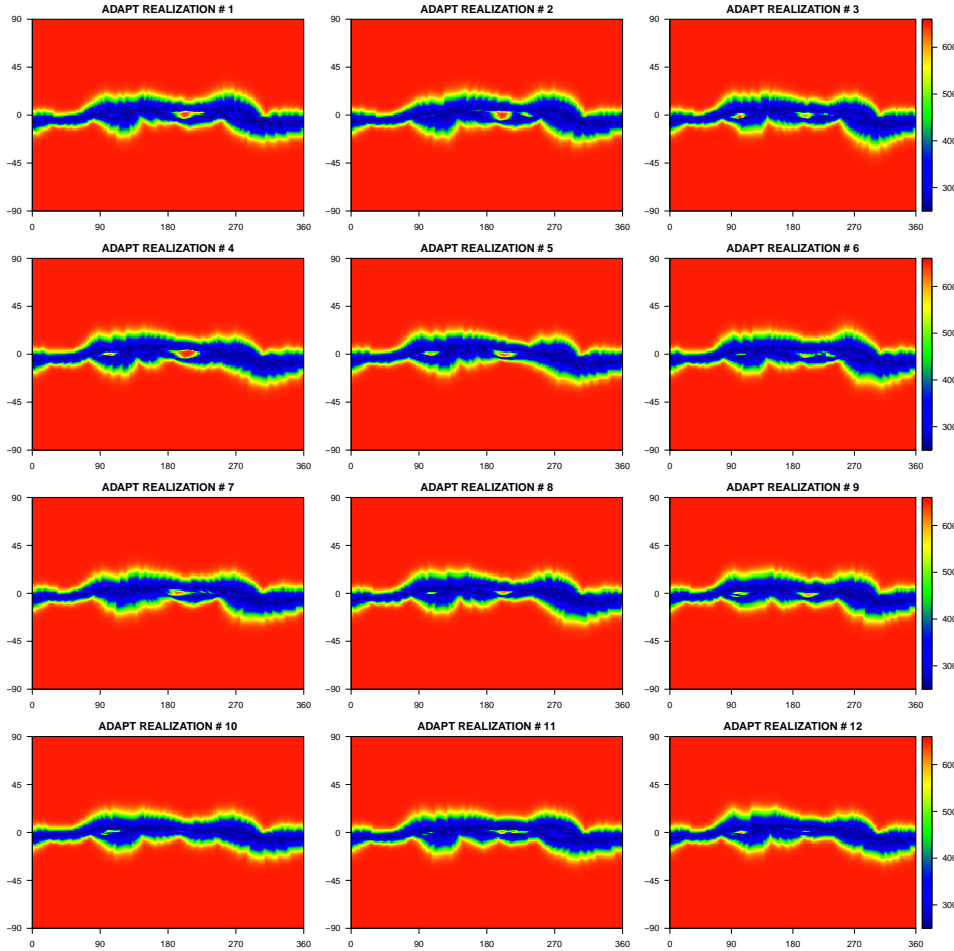
Our goal in this study is not to attempt to find the best match between models of ICMEs and their observed signatures, but, for a range of typical values, to assess how sensitive the ToA of the event at Earth is to the various input parameters used to launch the CME. For this reason, it is not necessary to run the most sophisticated numerical model. In fact, since the goal is to generate a large number of solutions to estimate uncertainties, we chose an empirical background model to generate the ambient solar wind [Riley *et al.*, 2001; Riley *et al.*, 2012]. In this approach, the magnetic field of the corona is computed using the observed photospheric field maps shown in Figure 1, and the structure of the field is used to generate the boundary conditions for the heliospheric simulation. In partic-



130 **Figure 1.** Twelve ADAPT Quasi-synchronic maps for Carrington rotation 2207. The panels have been  
 131 saturated at  $\pm 10$  G.

162 ular, we use the “Distance from the Coronal Hole” (DCHB) technique [Riley *et al.*,  
 163 2001] to generate longitude-latitude maps of solar wind speed at the inner boundary of the  
 164 heliospheric calculation (at  $30R_S$ ). The Radial component of the magnetic field is used  
 165 directly from the coronal solution, and the other (normal) components of the field and ve-  
 166 locity are set to zero. Pressure balance and momentum flux balance across the sphere at  
 167  $30R_S$  are used to specify the remaining magnetofluid parameters, temperature and den-  
 168 sity, respectively. This approach is similar in concept to that employed by WSA+ENLIL  
 169 [Pizzo *et al.*, 2015], except that WSA+ENLIL use expansion factor to specify the values  
 170 of solar wind speed at the inner radial boundary of the heliospheric model. Although we  
 171 have demonstrated that the DCHB method is generally more accurate than the WSA ap-  
 172 proach [Riley *et al.*, 2015], for the purposes of this investigation, either approach could be  
 173 justified.

176 Figure 2 shows the computed radial speed at the inner boundary of the heliospheric  
 177 calculation for the synchronic maps shown in Figure 1. We can make the same general  
 178 comments about the overall similarity between each of the panels, but again, note the  
 179 appearance of more subtle smaller-scale differences. In fact, these differences are more  
 180 noticeable in the boundary conditions for solar wind speed than they were for the photo-  
 181 spheric magnetic field, with the longitudinal alignment of fast-slow (or slow-fast) bound-  
 182 aries shifting by  $5\text{--}10^\circ$  in some cases. Additionally, the relative orientation (in the latitude-



174 **Figure 2.** Computed radial speed at the inner boundary of the heliospheric model for Carrington rotation  
 175 2207.

183 longitude plane) of the fast-slow boundaries changes from one realization to the next. Al-  
 184 though it is possible to infer how these differences will evolve (at least qualitatively) as the  
 185 plasma propagates away from the Sun, it is difficult, if not impossible to reliably deduce  
 186 how CME propagation (and deformation) will be affected by the differences.

### 187 2.2.2 CME Pulses

188 To mimic the launch of a CME from the upper corona, we follow the same prescrip-  
 189 tion as other forecasting teams, by specifying the location, direction, speed, temperature,  
 190 and density (or mass) of the ejecta as it passes through the inner radial boundary of the  
 191 simulation. For the purposes of brevity, we report here on the following permutations: (1)  
 192 Speed  $\hat{A}\hat{S}$  800, 1000, and 1200 km s<sup>-1</sup>; (2) Density  $\hat{A}\hat{S}$   $\times 1$ ,  $\times 2$ , and  $\times 4$  enhancement  
 193 over a background base density of 500 cm<sup>-3</sup>; and (3) Propagation direction/location  $\hat{A}\hat{S}$   
 194 100 radial traces within a 15° circle about the CME's launch center. The temperature  
 195 was assumed to be that of the ambient slow solar wind and the direction of propagation  
 196 was assumed to be radial. Taken together, these variations represent reasonable uncertain-  
 197 ties in the initial properties of CMEs observed in white light. The CME pulse is launched  
 198 by smoothly raising the variable's value over a one-hour interval, keeping it constant  
 199 for the next 12 hours, and then smoothly returning it to ambient values over a one-hour

200 interval. Although the precise shape of the CME’s profile can have a modest impact on  
 201 the resulting structure of the ICME farther out in the solar wind [e.g., *Riley and Gosling,*  
 202 1998], it does not impact the analysis presented here.

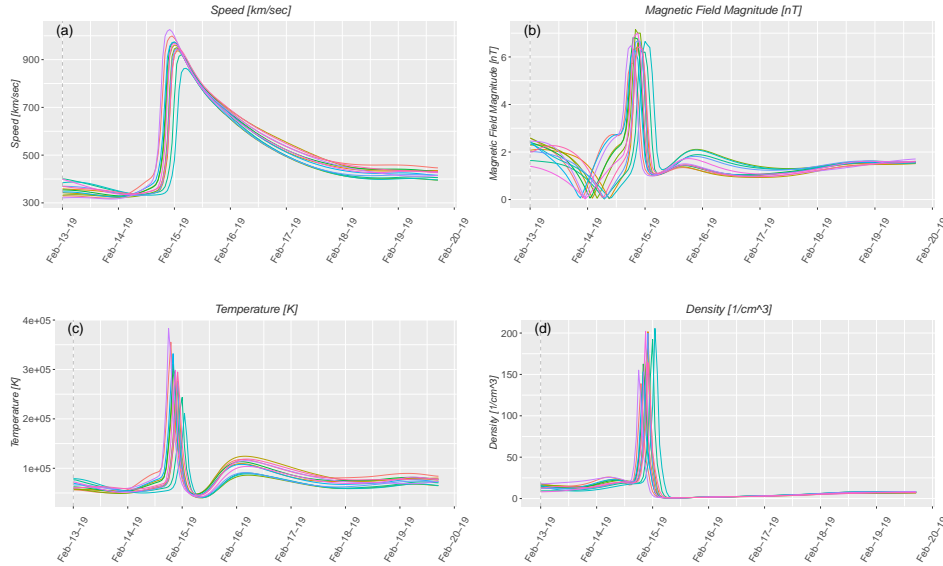
203 With three inputs each for speed and density, 100 values for “location”, and, for  
 204 all of these combinations, 12 realizations of the ambient solar wind, there are a total of  
 205 10,800 plausible time series that could be observed at Earth. Again, we reiterate that, as a  
 206 sensitivity study, there is no “ground truth” answer concerning which is the most correct,  
 207 only different clusters of results to estimate the relative contribution to uncertainties due  
 208 to our incomplete knowledge of the properties of the CME or the ambient solar wind into  
 209 which it is propagating.

210 Regarding the “location” variable, rather than simulating 100 events with slightly  
 211 different initial launch points in longitude and latitude ( $\phi, \lambda$ ), we took the more pragmatic  
 212 approach of flying hypothetical spacecraft through different parts of the ejecta, within a  
 213  $\pm 15^\circ$  cone of the CME center. Although strictly not the same, it effectively allows us to  
 214 generate multiple realizations for uncertainties in the relative position of the ICME to the  
 215 Earth. That is, rather than moving the ICME around, we are moving the Earth’s position  
 216 around to generate appropriate realizations.

### 217 3 Results

218 We begin by assessing the impact of the background solar wind on ToA uncertainty.  
 219 For each of the 12 realizations summarized in Figures 1 and 2, we launched an ICME  
 220 with a speed of  $1200 \text{ km s}^{-1}$  and a density twice that of the base value. Figure 3 shows  
 221 the resulting profiles measured at a hypothetical spacecraft located at  $r = 1 \text{ AU}$ ,  $\lambda = 0^\circ$ ,  
 222  $\phi = 180^\circ$ , that is, at the center of origin of the ICME. Several points are worth making.  
 223 First, ADAPT realizations have an important impact on the evolution of the ICME. Speed  
 224 measurements differ significantly with a peak as low as  $863 \text{ km s}^{-1}$  to as high as  $1026 \text{ km}$   
 225  $\text{s}^{-1}$ . This also affects the ToA of the leading edge of the CME disturbance, with the shock  
 226 arriving over a window of more than twelve hours. Similar variations are seen in the other  
 227 plasma and magnetic field parameters. The importance of this result cannot be overstated.  
 228 Given that each of these realizations is equally valid, we cannot distinguish between the  
 229 quality of the forecasts from each one. Thus, we infer that there is an intrinsic limitation  
 230 of  $\pm 7$  hours (the time separating the arrival of the first and last realization at a point one-  
 231 third of the way up the shock front) based only on our uncertainty in the magnetograms.  
 232 Moreover, this assumes that the magnetograms represent some kind of “ground truth”. In  
 233 reality, we know that there are substantially larger differences between synoptic maps gen-  
 234 erated from different solar observatories [*Riley et al., 2014*]. Thus, the true uncertainties  
 235 from the choice of magnetograms is likely larger.

239 We can also analyze the arrival time of the ejecta more precisely by adding tracer  
 240 particles into the simulation. That is, massless particles that are advected out with the so-  
 241 lar wind. By placing them at the leading edge of the CME pulse, we can accurately track  
 242 their arrival at 1 AU. Figure 4 summarizes the properties of the solar wind at 1 AU, again  
 243 in the equatorial plane. These are traces of the solar wind that started approximately two  
 244 days preceding the arrival of CME at Earth. Focusing first on the radial velocity, the am-  
 245 bient solar wind derived from the 12 ADAPT realizations can differ by approximately  $100$   
 246  $\text{km s}^{-1}$  at both high and low speeds. There are also substantial relative differences in both  
 247 tangential components of the field. Although it is tempting to conclude that, given the  
 248 large radial velocity of the CME, these velocities probably do not contribute significantly  
 249 to differences in arrival time, in fact they do. The dashed lines indicate the ToA for each  
 250 of the CMEs within each realization, leading to  $\sim \pm 2$  hours uncertainty in ToA. Note,  
 251 however, that the CME arrival times associated with the highest solar wind speed just  
 252 ahead of them are not always those that arrive first. This is probably related to the fact  
 253 that when tracking these tracer particles, they are not traveling out radially, but also re-

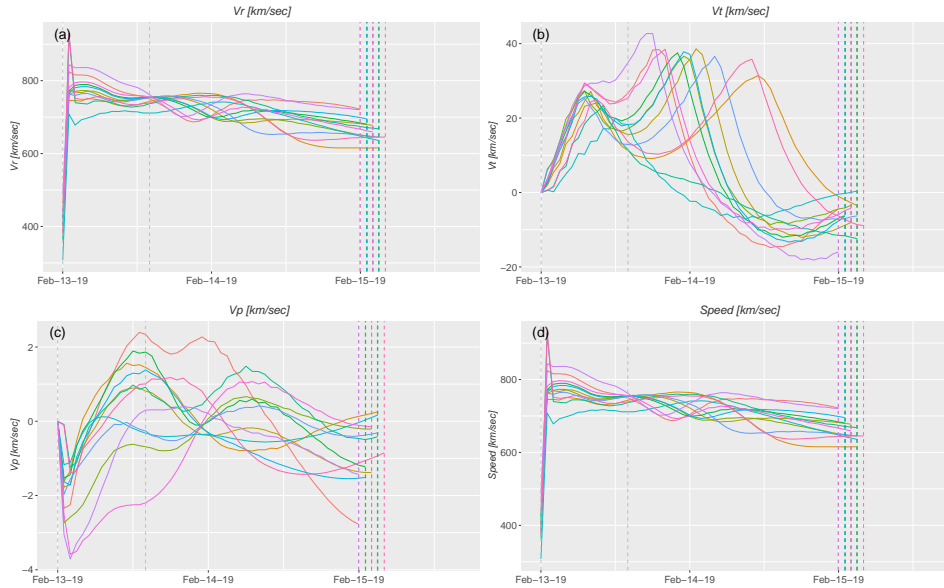


236 **Figure 3.** Solar wind profiles for a hypothetical CME launched into the solar wind conditions summarized  
 237 in Figure 2. The CME had an initial speed of  $1200 \text{ km s}^{-1}$  and a density twice that of the base value. The  
 238 dashed line marks the time that the CME was launched from the inner boundary.

254 sponding to shearing flows that move them in the transverse direction. Finally, it is worth  
 255 noting that the uncertainty in ToA computed for the tracer particles ( $\pm 2$  hours) is notably  
 256 smaller than those estimated from the time of arrival of the CME shock ( $\pm 7$  hours). In the  
 257 former case, we are estimating ToA based on the time history of the particle as it advects  
 258 through the solar wind, while in the latter, we are identifying the ToA from the passage of  
 259 a shock (or steepened wave) across the observer’s position. Given the non-radial flow,  
 260 it is possible that this plasma is laterally separated significantly from the parcel of plasma  
 261 that launched at the CME’s leading-edge center.

265 A final point worth making about the profiles in Figure 4 is that, despite the large  
 266 variations upstream of the ICME from different realizations, none of the plasma shown  
 267 from February 13 through to early February 15 have any impact upon the ToA of the  
 268 ICME disturbance nor the deformation of its large-scale structure. Only the plasma di-  
 269 rectly ahead of the CME can interact with the CME pulse, and, by definition, this is lim-  
 270 ited to the region downstream of the fast-mode forward shock. Thus, while it is crucial to  
 271 estimate the properties of the ambient solar wind near to, or surrounding the CME struc-  
 272 ture, the details of the solar wind away from this region matter little from a forecasting  
 273 perspective. Of course, currently, there is no way to disentangle the two: large-scale mod-  
 274 els require global, or near global geometries. Moreover, the properties of the ambient so-  
 275 lar wind in the ecliptic plane are modulated, to a large degree, by the properties of the  
 276 polar magnetic field [Riley *et al.*, 2019] making it less likely that simpler 1-D or 2-D ad  
 277 hoc approaches can accurately forecast the ambient solar wind into which the CME will  
 278 be embedded and interact with.

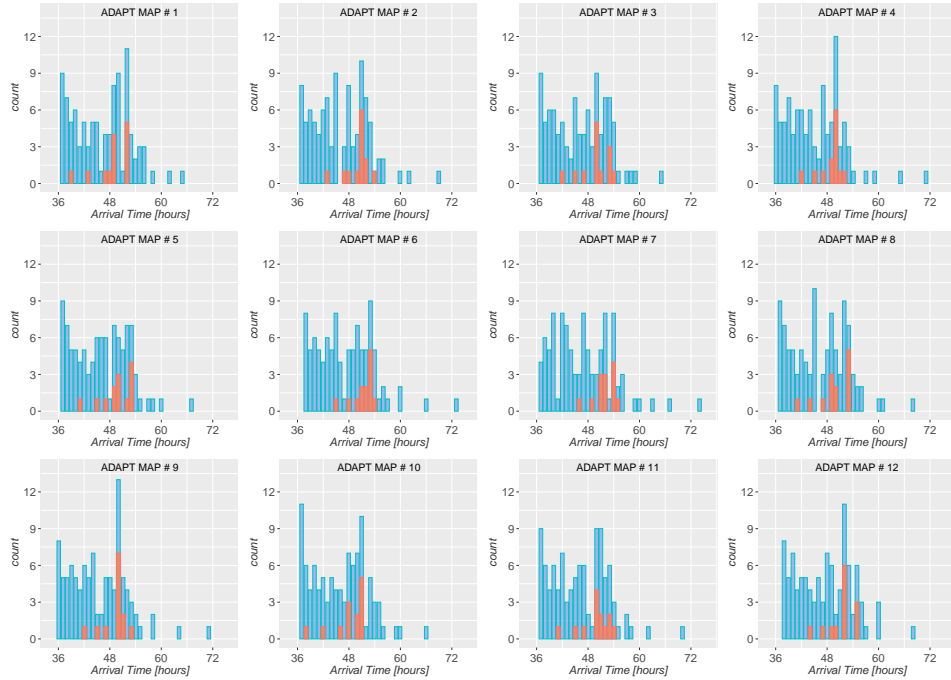
279 Next, we estimate the impact of uncertainties in the ToA of CMEs based on errors  
 280 in our estimation of the propagation direction of the CME. Even when multiple spacecraft  
 281 observe the same event, it is unlikely that the true direction is known to within  $5 - 15^\circ$ .  
 282 As noted above, rather than running a suite of events where we launch an otherwise iden-  
 283 tical CME in slightly different directions, we can mimic the effect by following the loci  
 284 of tracer particles within the CME that are spread out by a similar transverse amount,



262 **Figure 4.** Upstream velocity components (in spherical coordinates:  $v_r, v_\theta, v_\phi$ ) for the ambient solar wind  
 263 realizations shown in Figure 2. The arrival of the ICME propagating through these solutions is indicated by  
 264 the dashed vertical lines.

285 as shown in Figure 5. The two distributions (blue and red) encapsulate the worst ( $\pm 15^\circ$ )  
 286 and best ( $\pm 5^\circ$ ) forecast predictions, respectively, based on either one set of coronal ob-  
 287 servations to constrain the CME, or multiple observations from more than one space-  
 288 craft. In the worst case, with only observations from, say, Earth, it is likely that the CME  
 289 ToA could be forecast to be between 40 and 59 hours. Or, equivalently,  $\pm 9.5$  hours (us-  
 290 ing 5/95% quantiles). This is similar to the uncertainties prevalent in current forecasts  
 291 of the ToA of ICMEs [Riley *et al.*, 2018]. If the uncertainties in initial direction can be  
 292 constrained to within  $\pm 5^\circ$ , the associated errors in ToA are substantially reduced, say, be-  
 293 tween 44 and 58 hours, or 5/95% CI:  $\pm 7$  hours. (For comparison, using mean values and  
 294 standard deviations would lead to estimates of: 41/55 or  $\pm 7$  hours and 50/58 or  $\pm 4$  hours,  
 295 respectively).

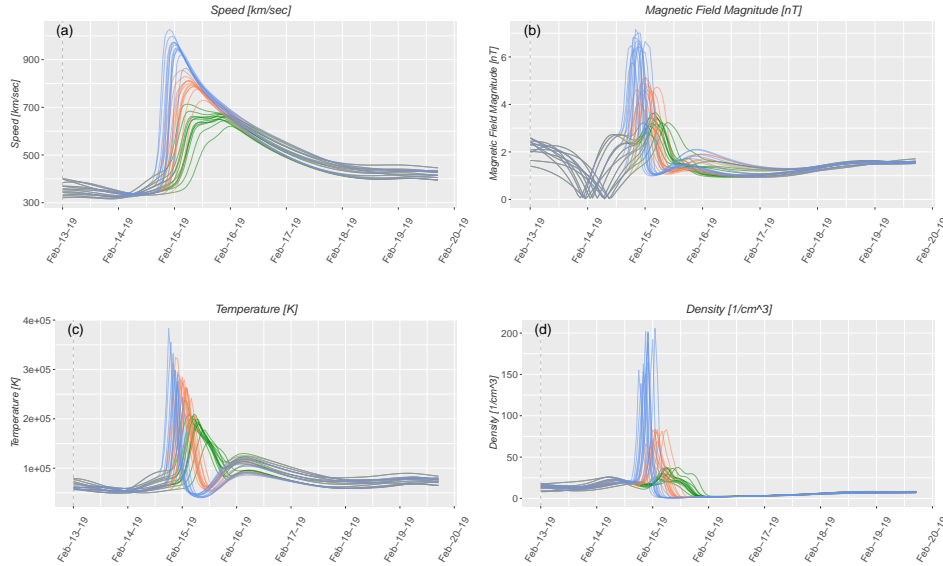
299 We also investigated how uncertainties in the ToA of ICMEs depended on the ini-  
 300 tial speed of the ICME, which is generally only known to within  $\pm 200 \text{ km s}^{-1}$ , but again  
 301 dependent on the number and quality of the observations used to derive that estimate. As  
 302 summarized in Figure 6, we visually infer that for a CME traveling at 1200, 1000, and  
 303  $800 \text{ km s}^{-1}$ , the ToA of the first tracer particle was delayed by approximately 4 hours for  
 304 each  $200 \text{ km s}^{-1}$  drop in initial speed. More quantitatively, we computed the mean, me-  
 305 dian, range, s.d. and 5/95% CIs for the point where the speed exceeded  $500 \text{ km s}^{-1}$  (i.e.,  
 306 on the early ascending portion of the shock front). As an example, the median ToA for  
 307 the 800, 1000, and  $1200 \text{ km s}^{-1}$  ICME was 690, 390, and 210 minutes, respectively. From  
 308 this, we can infer that the average uncertainty was 180 and 300 minutes between succes-  
 309 sive ICMEs, or in total, 8 hours. Thus, we conclude that (at least for this event) if the  
 310 speed is known to only within  $\pm 200 \text{ km s}^{-1}$ , the associated uncertainty in ToA is  $\sim \pm 4$   
 311 hours. Comparing the traces, we can make several remarks. First, prior to the arrival of  
 312 the shock, all profiles are the same, that is, the only variability is due to the ADAPT real-  
 313 izations. Second, the compression region driven by the speed increase, and visible in the  
 314 field magnitude, temperature, and density, is centered on the initial speed gradient and,  
 315 thus, is staggered in time in relation to the phasing of the shock location. Third, the am-  
 316 plitude of the compression is in proportion to the jump in speed, although the fractional



296 **Figure 5.** Histogram of arrival times for a set of tracer particles embedded at the leading edge of the cone-  
 297 model CME. The larger (blue) group were all within  $\pm 15^\circ$  of center, while the smaller (red) group were all  
 298 within  $\pm 5^\circ$  of the center.

317 change above background values increases from one parameter to the next, with density  
 318 showing a more than doubling between each of the velocity pulses. Fourth, the rarefaction  
 319 created on the declining speed profile is proportionately longer for the faster ICME, but  
 320 the trailing edge of this wave merges into the background flow at roughly the same time  
 321 for each case. Fifth, the spread in the ToA of the shock front due to (1) the different re-  
 322 realizations (clusters of profiles of the same colors) and (2) the different initial speed jumps  
 323 (sequential profiles of different colors) are of approximately the same magnitude, suggest-  
 324 ing that these sources of uncertainty are roughly comparable.

325 Finally, it is well appreciated that the mass of the CME is one of the most difficult  
 326 properties to determine with any degree of accuracy [e.g., *Vourlidas et al., 2010*]. To ex-  
 327 plore what kind of impact this might have, we considered the effects of doubling (or halv-  
 328 ing) the initial mass within the ejecta. Using the same analysis as described above for un-  
 329 certainties in CME speed, we found that the difference for mass uncertainties was more  
 330 modest;  $\sim \pm 2.5$  hours separated each ICME profile for a given ambient solar wind re-  
 331 realization (Figure 7). Visually, given the fact that the profiles of different colors overlap  
 332 much more, it is clear that the choice of ADAPT realization has a much larger impact on  
 333 the ToA than the inferred mass of the CME. However, it is quite conceivable that mass  
 334 uncertainties are larger than the factor of two assumed here. Unfortunately, even this un-  
 335 certainty is “uncertain.” In comparison with Figure 6, we also note that modifying  
 336 the mass of the ICME does not generate the same variations in the structure of the events.  
 337 That is, ICMEs of the same speed, differing only in mass, produce more dynamically simi-  
 338 lar events. More massive events arrive sooner, have a modestly higher peak speed, field  
 339 strength, temperature, and density, but do not have unique features, such as the erosion in  
 340 peak speed seen in the case of the  $800 \text{ km s}^{-1}$  event in Figure 6.



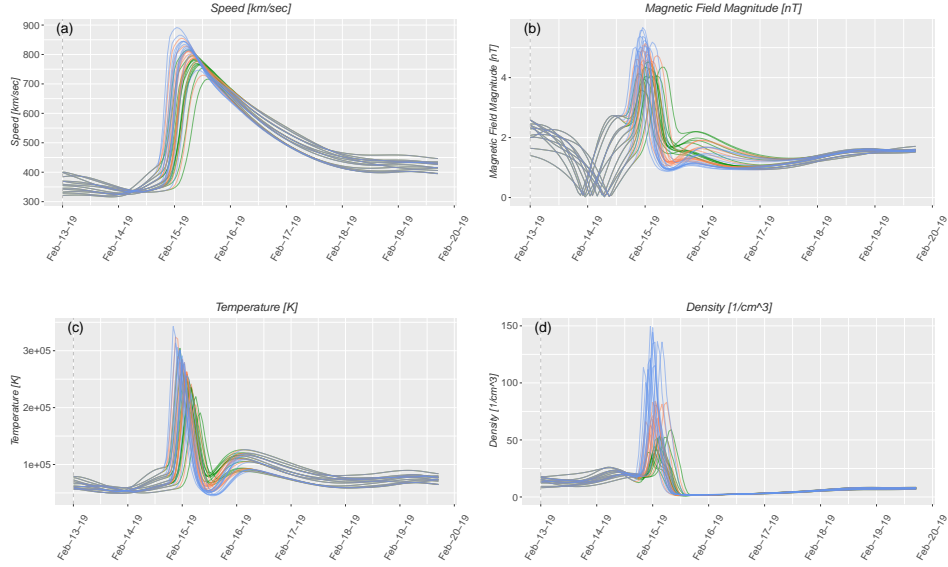
341 **Figure 6.** Comparison of arrival times for ICMEs with speeds 800 (green), 1000 (red), and 1200 (blue) km  
 342  $s^{-1}$ : (a) Speed; (b) magnetic field magnitude; (c) temperature; and (d) density.

#### 346 4 Conclusions and Discussion

347 In this study, we have investigated the main sources of error in predicting a CME’s  
 348 ToA at Earth: (1) the initial properties of the ejecta, including its speed, mass, and direc-  
 349 tion of propagation; and (2) the properties of the ambient solar wind into which it propa-  
 350 gates. To estimate the relative contribution to ToA errors, we constructed a set of nu-  
 351 merical experiments of cone-model CMEs where we varied the initial speed, mass, and  
 352 direction of the ejecta at the inner heliospheric boundary. Additionally, we built an en-  
 353 semble of 12 ambient solar wind solutions using realizations from the Air Force’s ADAPT  
 354 model. We found that each point of uncertainty contributed between  $\pm 2.5$  to  $\pm 7$  hours of  
 355 uncertainty to the estimate of the CME’s ToA. Importantly, different realizations of the  
 356 input magnetic synoptic maps resulted in errors of a similar magnitude, suggesting that  
 357 estimates of ToA will continue to be plagued with intrinsic errors of  $\sim \pm 10$  hours until  
 358 tighter constraints can be found for these boundary conditions, which will likely require  
 359 more comprehensive observations of the Sun. Finally, our results suggest that there are  
 360 clear benefits to focused investigations aimed at reducing the uncertainties in: CME speed,  
 361 mass, direction, and input boundary magnetic fields.

362 Our results explain – to a large degree – the errors found in the forecasts made for  
 363 the CCMC’s “CME Arrival Time Scoreboard” [Riley *et al.*, 2018]. A combination of un-  
 364 certainties in CME speed, direction, and mass, as well as uncertainties in the structure of  
 365 the background solar wind into which the CME is propagating all appear to contribute  
 366 to varying degrees. It is not surprising, therefore, that none of the models can make esti-  
 367 mates where the MAE is smaller than about 12 hours. It is worth noting, however, that  
 368 different models tend to focus on different aspects of the forecasting pipeline. Thus, it  
 369 may be possible to combine the best practices from different techniques and improve skill  
 370 scores, at least modestly.

371 Uncertainties in the properties of the ambient solar wind were shown to have a sig-  
 372 nificant effect in the arrival time of the CME at Earth, in spite of the fact that our analysis  
 373 was based on only modest differences between each of the 12 realizations calculated for



343 **Figure 7.** Comparison of arrival times for ICMEs density enhancements of  $\times 1$  (green),  $\times 2$  (red), and  $\times 4$   
 344 (blue) above background for, a  $1000 \text{ km s}^{-1}$  CME: (a) Speed; (b) magnetic field magnitude; (c) temperature;  
 345 and (d) density.

374 one ADAPT map. As we have demonstrated previously [Riley *et al.*, 2014, 2012], forecasts  
 375 using magnetogram data from different solar observatories will further increase the differ-  
 376 ences in the properties of the ambient solar wind, and hence, lead to even larger dispar-  
 377 ities in the arrival time of the ICME at Earth. These errors, can only be fully addressed  
 378 by new, comprehensive observations of the Sun that, ideally, would cover  $4\pi$  steradians  
 379 of the solar surface. In practice, such a mission would require at least two polar orbiting  
 380 spacecraft, together with at least three near-ecliptic spacecraft [Riley *et al.*, 2006]. In lieu  
 381 of that, we suggest that modest gains may be obtained from improvements to the data as-  
 382 similation procedure in the ADAPT map pipeline. A crucial aspect of this would be the  
 383 extrapolation and “filling in” of missing polar observations, which are key for improving  
 384 forecasts, even in the ecliptic plane [Riley *et al.*, 2019].

385 Uncertainties in CME speed, direction, and mass also resulted in significant errors  
 386 in arrival time. Ultimately, we believe that first-principles models, which include the erup-  
 387 tion of the CME and its propagation through the low corona, will produce the most ac-  
 388 curate forecasts; however, in analogy with meteorological advances in the 1980s and  
 389 1990s, our understanding of the system has not matured to the point that these mod-  
 390 els can outperform empirical models. Thus, near-term advances will likely come from  
 391 constraining the properties of the ejecta in the high corona. Analysis of multi-spacecraft  
 392 white-light observations suggests that this approach can produce more accurate estimates  
 393 of the initial properties of the CME than single-spacecraft observations, although this has  
 394 not yet been demonstrated against global MHD simulations, for which there is an albeit  
 395 idealized “ground truth”.

396 Our results are broadly consistent with those of Pizzo *et al.* [2015], who found that  
 397 different solutions produced deterministic (non-chaotic) estimates for ToA. Additionally,  
 398 while we cannot quantitatively compare the dispersion in ToAs directly, the qualitative  
 399 spread of their results is consistent with ours (compare their Figures 10, 11, 14, and 16  
 400 with our Figures 3 - 7). Our study also provides an independent assessment that the re-  
 401 sults of Pizzo *et al.* [2015] are insensitive to any specific aspects of the forecasting pro-

402 cess, including: (1) the particular numerical model being used; (2) the resolution of the  
 403 simulations; (3) the empirical prescription of the ambient solar wind; (4) the choice of  
 404 time period under study; and (5) the specification and values of the CME pulses. How-  
 405 ever, our results extend the *Pizzo et al.* [2015] study in several important ways. First, we  
 406 drove the CMEs through realistic ambient backgrounds, modeled using realizations of the  
 407 observed photospheric magnetic field. Second, we considered uncertainties in the CME  
 408 pulse profiles that were based on the likely observation errors associated with estimating  
 409 these parameters (speed, location, and mass) from white-light measurements. And third,  
 410 we quantified the errors associated with each component in the modeling chain from the  
 411 Sun to the Earth.

412 This study is not, however, without limitations or caveats. First, we relied on a global  
 413 heliospheric MHD algorithm to compute the evolution of the ICME from near the Sun to  
 414 1 AU. While the accuracy of such codes has been tested and validated over the years, it is  
 415 worth noting that these algorithms tend to be numerically diffusive and, as such, tend to  
 416 dissipate small-scale fluctuations. This likely leads to structures that are more laminar than  
 417 would be observed. In terms of the results presented here, this would reduce the differ-  
 418 ences in ToA. Thus, the model results probably underestimate the spread in ToA. Second,  
 419 and as already noted, our choice of 12 ADAPT realizations also provides a lower limit on  
 420 the uncertainty in the magnetograms used to drive the ambient solar wind. Both differ-  
 421 ences in the actual numerical values of the flux as well as how regions that are not well  
 422 observed (limbs, far-side, and poles) are assembled would produce even greater variability  
 423 in the maps driving the ambient solutions. Third, our prescription of the CME was limited  
 424 to a simple hydrodynamic pulse. While this represents the current “state-of-the-art”,  
 425 observed CMEs clearly have a strong and significant magnetic structure embedded within  
 426 them. Thus, once models are capable of reliably incorporating flux rope structures, this  
 427 will result in an additional degree of uncertainty, dependent on how the properties of the  
 428 flux rope can be constrained. Fourth, CMEs are often associated with precursor events  
 429 [e.g., *Gopalswamy et al.*, 2001]. This is particularly true for fast, and hence more geo-  
 430 effective events. These can either provide a means for sweeping out ambient solar wind  
 431 structure ahead of the CME under consideration, or act as an obstacle that the following  
 432 CME interacts with. In either case, this added complexity will also act to disperse the pre-  
 433 dicted ToAs, that is, it will increase the uncertainty in the forecasts.

434 In this study, by design, we did not study an observed event. We were not attempt-  
 435 ing to uncover the “correct” answer. Instead, our goal was to quantify the sources of un-  
 436 certainty in the ToA of CMEs. Forecasting observed events is, ultimately, a more impor-  
 437 tant objective. However, in the case of predicting observed events, care must be taken to  
 438 avoid biasing the results by adjusting input parameters to more closely match the observa-  
 439 tions. True forecasts, such as those submitted to the CCMC’s “CME Arrival Time Score-  
 440 board” avoid this problem by requiring submissions prior to the arrival of the CME at  
 441 1 AU. On the other hand, hindcasts, or “retrospective forecasts” can potentially result in  
 442 overly-optimistic results, since the analyst may (inadvertently) adjust input parameters to  
 443 improve the forecast, in which case, the forecast is more of a curve fitting exercise than  
 444 a demonstration of a promising technique. Nevertheless, when applied over a sufficiently  
 445 large number of events, this could provide important information for constraining the free  
 446 parameters of the model. The final test, however, remains to predict future events, such as  
 447 through the CCMC portal, and this should be an objective for any ICME forecasting tool.  
 448 In the interim, rigorous hindcast exercises could be conducted using the events catalogued  
 449 at the CCMC portal, together with code made available to compare the new model’s re-  
 450 sults with those that originally made the forecasts [*Riley et al.*, 2018].

451 In closing, based on the results presented here, we suggest that there are fundamen-  
 452 tal limitations to the accuracy that current CME forecasting tools can achieve. Modest ad-  
 453 vances can be made by more thorough analyses, including comprehensive efforts to ‘hind-  
 454 cast’ many ICME events and use robust statistical approaches to better constrain free pa-

455 rameters. However, ultimately, the greatest improvements will only come from a substan-  
 456 tial investment in the form of multi-viewpoint observations of the photospheric magnetic  
 457 field and white-light images of the corona.

## 458 Acknowledgments

459 The authors gratefully acknowledge support from NASA (80NSSC18K0100, NNX16AG86G,  
 460 80NSSC18K1129, 80NSSC18K0101, 80NSSC20K1285, 80NSSC18K1201, and NNN06AA01C),  
 461 NOAA (NA18NWS4680081), and the U.S. Air Force (FA9550-15-C-0001).

462 All model results analyzed in this study are (or will soon be) available from the fol-  
 463 lowing repository: Riley and Ben-Nun (2021b). In the interim, they can be downloaded  
 464 from [www.predsci.com/~pete/research/riley-ben-nun-2021a/](http://www.predsci.com/~pete/research/riley-ben-nun-2021a/).

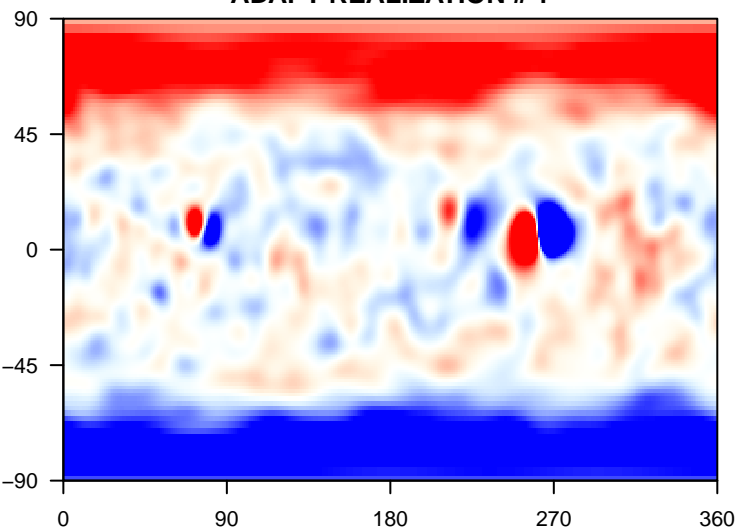
## 465 References

- 466 Arge, C. N., D. Odstrcil, V. J. Pizzo, and L. R. Mayer (2003), Improved Method for Spec-  
 467 ifying Solar Wind Speed Near the Sun, in *Solar Wind Ten, American Institute of Physics*  
 468 *Conference Series*, vol. 679, edited by M. Velli, R. Bruno, F. Malara, and B. Bucci, pp.  
 469 190–193, doi:10.1063/1.1618574.
- 470 Arge, C. N., C. J. Henney, J. Koller, C. R. Compeau, S. Young, D. MacKenzie, A. Fay,  
 471 and J. W. Harvey (2010), Air Force data assimilative photospheric flux transport  
 472 (ADAPT) Model. In: Maksimovic, M., Issautier, K., Meyer-Vernet, N., Moncuquet, M.,  
 473 Pantellini, F. (eds.), *Twelfth International Solar Wind Conference, AIP Conf. Proc.*, 1216,  
 474 343–346, doi:10.1063/1.3395870.
- 475 Forbes, T. G., and J. Lin (2000), What can we learn about reconnection from coronal  
 476 mass ejections, *J. Atmos. Sol.-Terr. Phys.*, 62, 1499–1507.
- 477 Gopalswamy, N., S. Yashiro, M. L. Kaiser, R. A. Howard, and J. L. Boueret (2001), Radio  
 478 signatures of coronal mass ejection interaction: Coronal mass ejection cannibalism?,  
 479 *Astrophys. J.*, 548(1), L91–L94.
- 480 Gosling, J. T., S. J. Bame, D. J. McComas, and J. L. Phillips (1990), Coronal mass ejec-  
 481 tions and large geomagnetic storms, *Geophys. Res. Lett.*, 17, 901.
- 482 Mays, M., A. Taktakishvili, A. Pulkkinen, P. MacNeice, L. Rastätter, D. Odstrcil, L. Jian,  
 483 I. Richardson, J. LaSota, Y. Zheng, et al. (2015), Ensemble modeling of cmes using the  
 484 wsa-enlil+ cone model, *Solar Physics*, 290(6), 1775–1814.
- 485 Odstrcil, D., P. Riley, J. A. Linker, R. Lionello, Z. Mikic, and V. J. Pizzo (2003), 3-D  
 486 simulations of ICMEs by coupled coronal and heliospheric models, in *ESA SP-535: So-*  
 487 *lar Variability as an Input to the Earth's Environment*, pp. 541–+.
- 488 Odstrcil, D., P. Riley, and X. P. Zhao (2004), Numerical simulation of the 12 May 1997  
 489 interplanetary CME event, *J. Geophys. Res.*, 109, 2116–+, doi:10.1029/2003JA010135.
- 490 Pizzo, V., G. Millward, A. Parsons, D. Biesecker, S. Hill, and D. Odstrcil (2011), Wang-  
 491 Sheeley-Arge-Enlil Cone Model Transitions to Operations, *Space Weather*, 9, 03004,  
 492 doi:10.1029/2011SW000663.
- 493 Pizzo, V., C. Koning, M. Cash, G. Millward, D. Biesecker, L. Puga, M. Codrescu, and  
 494 D. Odstrcil (2015), Theoretical basis for operational ensemble forecasting of coronal  
 495 mass ejections, *Space Weather*, 13(10), 676–697.
- 496 Riley, P., and J. T. Gosling (1998), Do coronal mass ejections implode in the solar wind?,  
 497 *Geophys. Res. Lett.*, 25, 1529.
- 498 Riley, P., J. A. Linker, and Z. Mikić (2001), An empirically-driven global MHD model  
 499 of the corona and inner heliosphere, *J. Geophys. Res.*, 106, 15,889, doi:10.1029/  
 500 2000JA000121.
- 501 Riley, P., J. A. Linker, Z. Mikić, D. Odstrcil, T. H. Zurbuchen, D. Lario, and R. P. Lep-  
 502 ping (2003), Using an MHD simulation to interpret the global context of a coronal mass  
 503 ejection observed by two spacecraft, *J. Geophys. Res.*, 108, 1272.

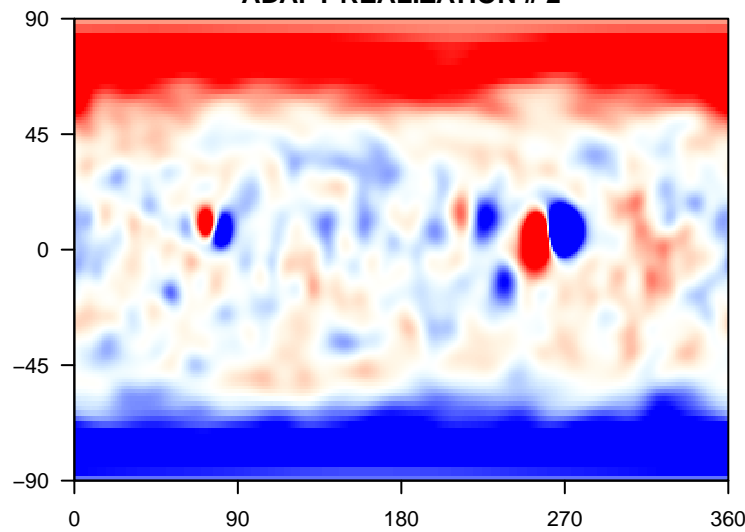
- 504 Riley, P., J. A. Linker, Z. Mikic, and R. Lionello (2006), Maximizing the Scientific Return  
505 of the Sentinels Mission using Global MHD Models, *AGU Fall Meeting Abstracts*, pp.  
506 C4+.
- 507 Riley, P., J. A. Linker, R. Lionello, and Z. Mikic (2012), Corotating interaction regions  
508 during the recent solar minimum: The power and limitations of global MHD modeling,  
509 *J. Atmos. Solar-Terr. Phys.*, *83*, 1–10, doi:10.1016/j.jastp.2011.12.013.
- 510 Riley, P., M. Ben-Nun, J. A. Linker, Z. Mikic, L. Svalgaard, J. Harvey, L. Bertello,  
511 T. Hoeksema, Y. Liu, and R. Ulrich (2014), A Multi-Observatory Inter-Comparison of  
512 Line-of-Sight Synoptic Solar Magnetograms, *Sol. Phys.*, *289*, 769–792, doi:10.1007/  
513 s11207-013-0353-1.
- 514 Riley, P., J. A. Linker, and C. N. Arge (2015), On the role played by magnetic expansion  
515 factor in the prediction of solar wind speed, *Space Weather*, *13*(3), 154–169.
- 516 Riley, P., M. L. Mays, J. Andries, T. Amerstorfer, D. Biesecker, V. Delouille, M. Dum-  
517 bović, X. Feng, E. Henley, J. A. Linker, et al. (2018), Forecasting the arrival time of  
518 coronal mass ejections: Analysis of the ccmc cme scoreboard, *Space Weather*, *16*(9),  
519 1245–1260.
- 520 Riley, P., J. A. Linker, Z. Mikic, R. M. Caplan, C. Downs, and J.-L. Thumm (2019), Can  
521 an unobserved concentration of magnetic flux above the poles of the sun resolve the  
522 open flux problem?, *The Astrophysical Journal*, *884*(1), 18.
- 523 Török, T., C. Downs, J. A. Linker, R. Lionello, V. S. Titov, Z. Mikić, P. Riley, R. M.  
524 Caplan, and J. Wijaya (2018), Sun-to-earth mhd simulation of the 2000 July 14  
525 “Bastille day” eruption, *The Astrophysical Journal*, *856*(1), 75.
- 526 Vourlidas, A., R. A. Howard, E. Esfandiari, S. Patsourakos, S. Yashiro, and G. Michalek  
527 (2010), Comprehensive analysis of coronal mass ejection mass and energy properties  
528 over a full solar cycle, *The Astrophysical Journal*, *722*(2), 1522.

**Figure.**

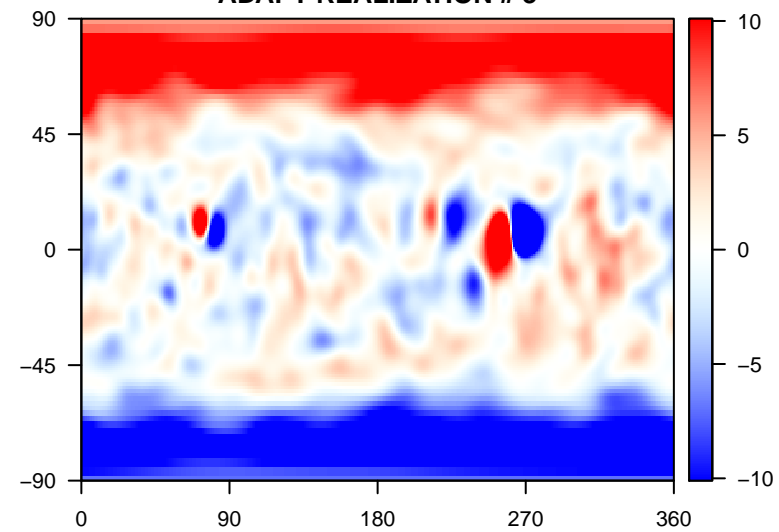
ADAPT REALIZATION # 1



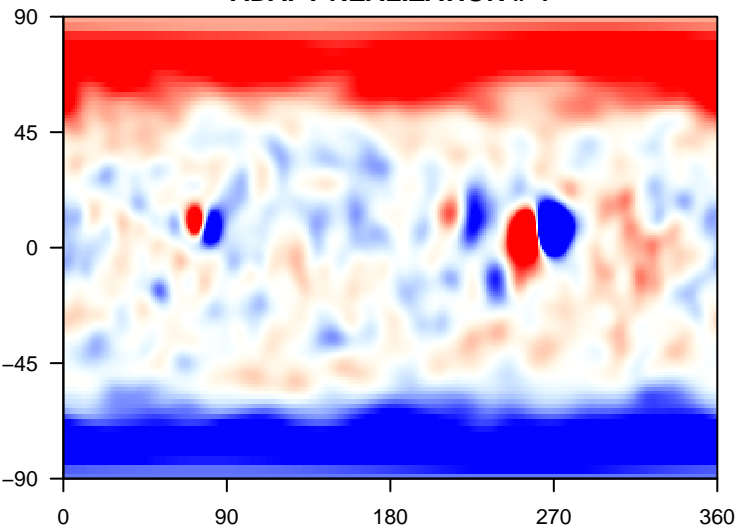
ADAPT REALIZATION # 2



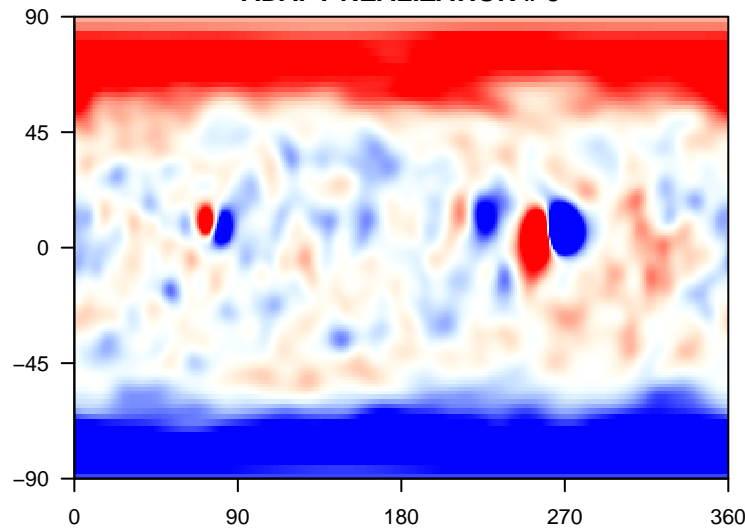
ADAPT REALIZATION # 3



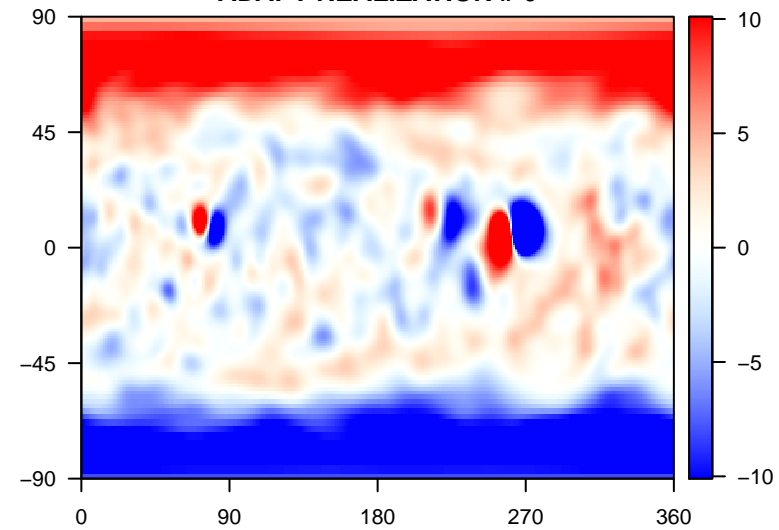
ADAPT REALIZATION # 4



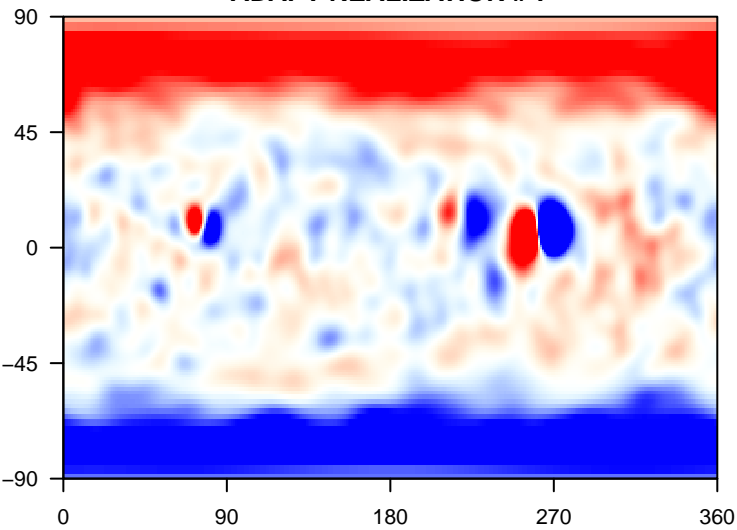
ADAPT REALIZATION # 5



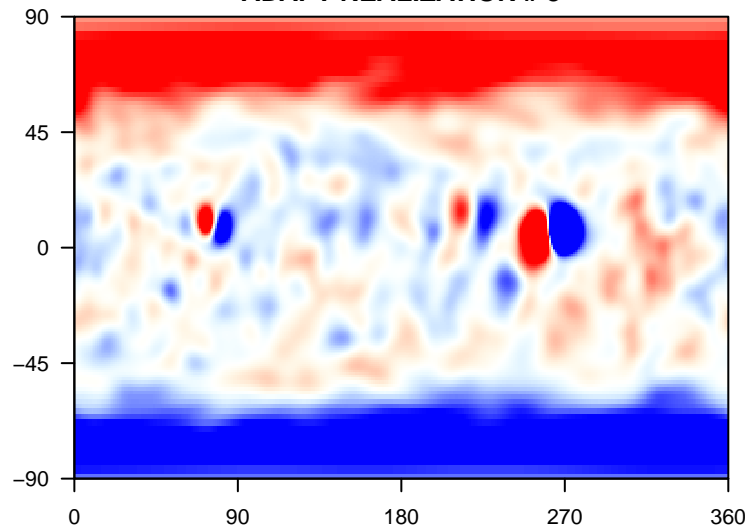
ADAPT REALIZATION # 6



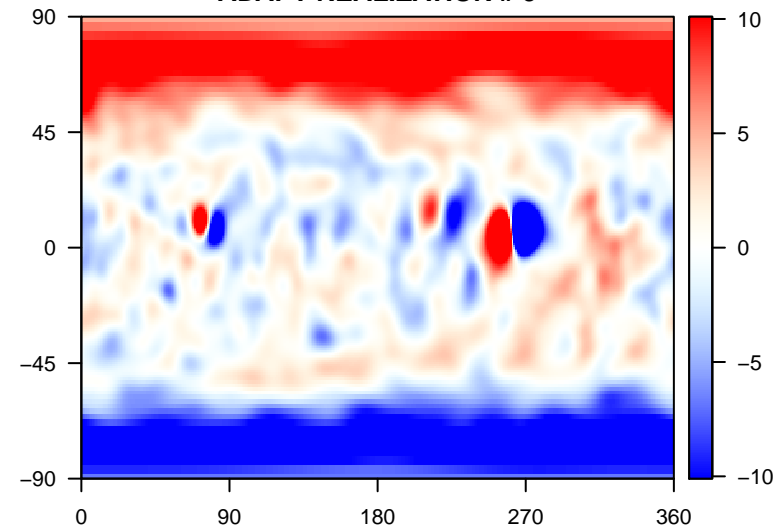
ADAPT REALIZATION # 7



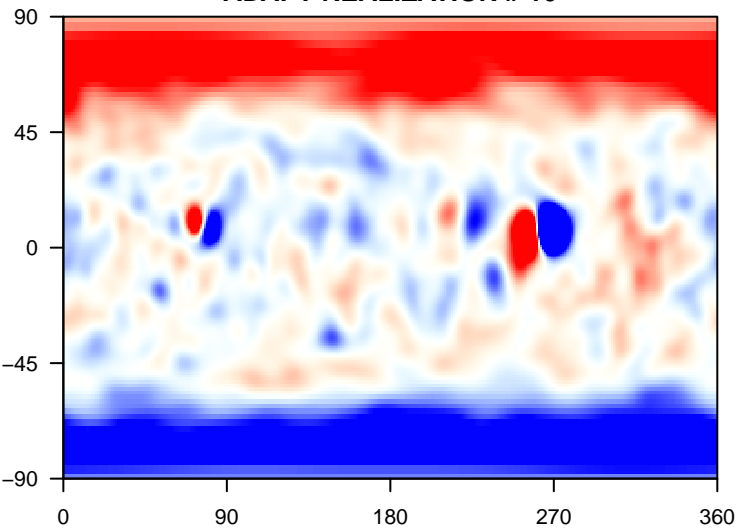
ADAPT REALIZATION # 8



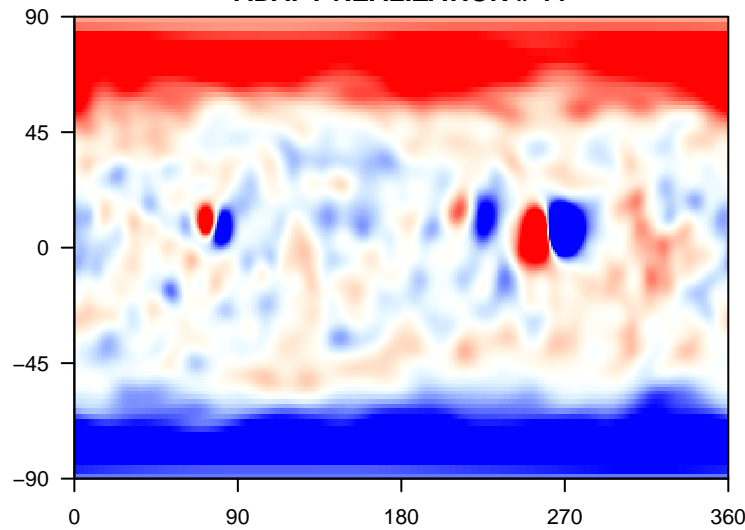
ADAPT REALIZATION # 9



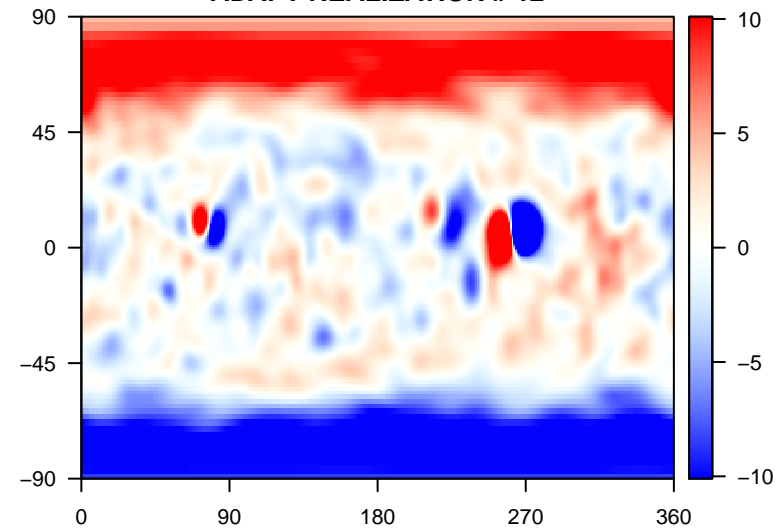
ADAPT REALIZATION # 10



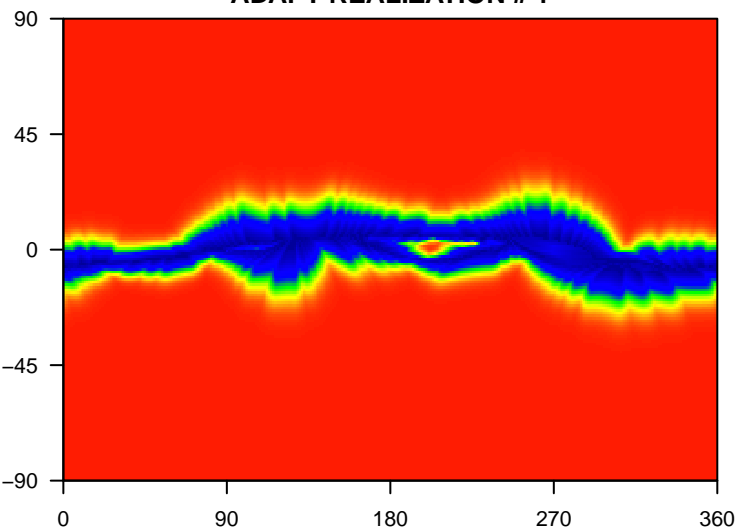
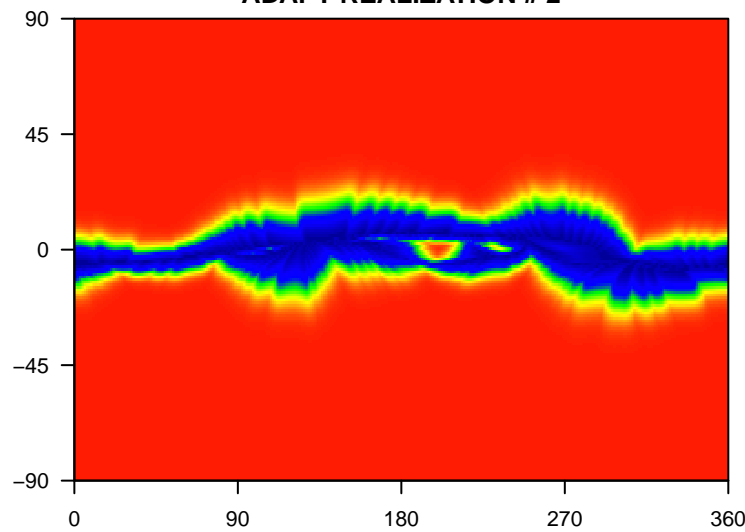
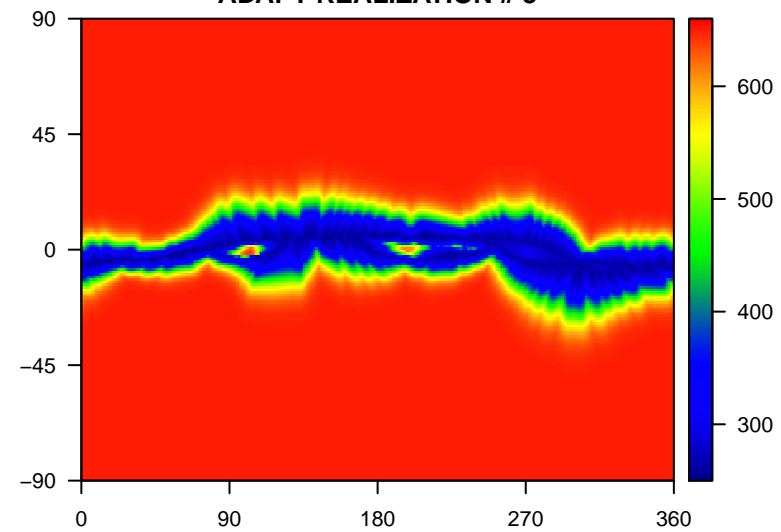
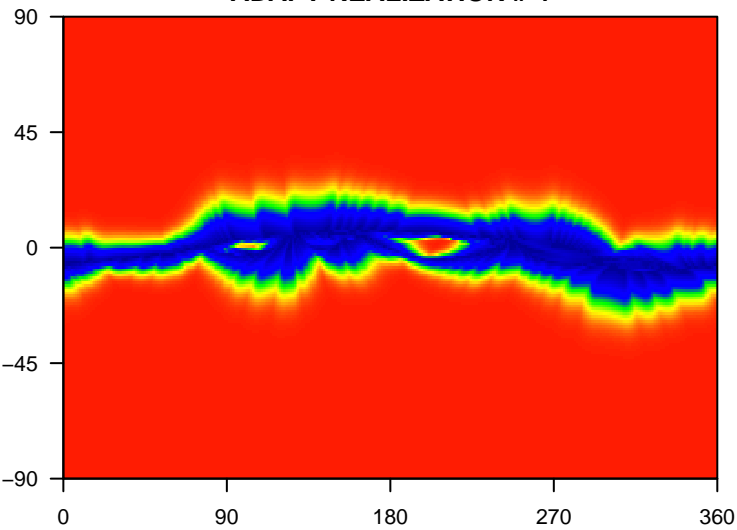
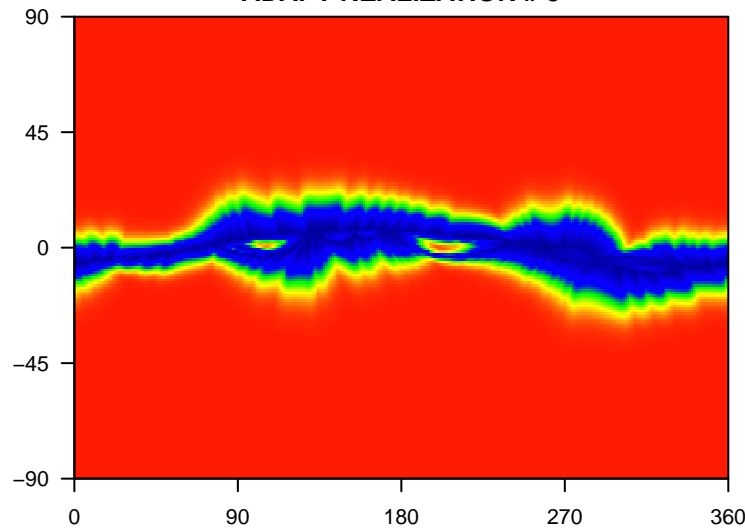
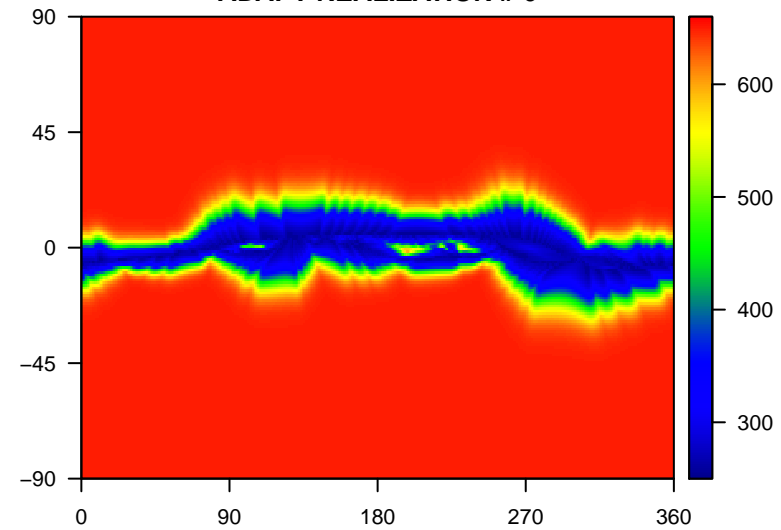
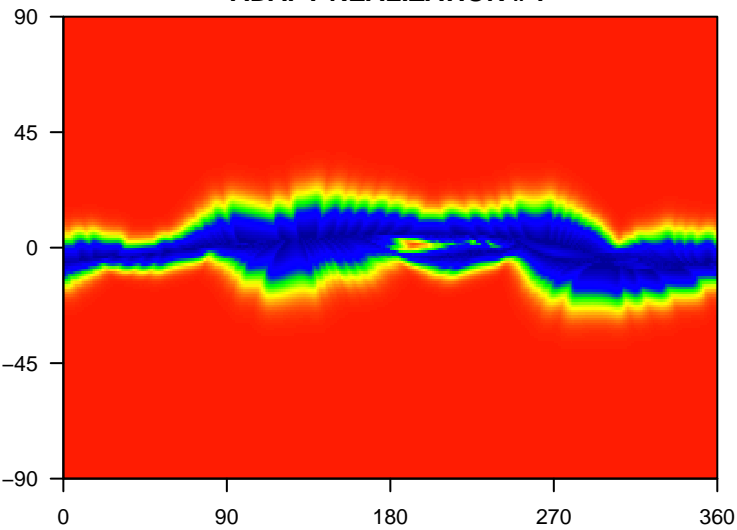
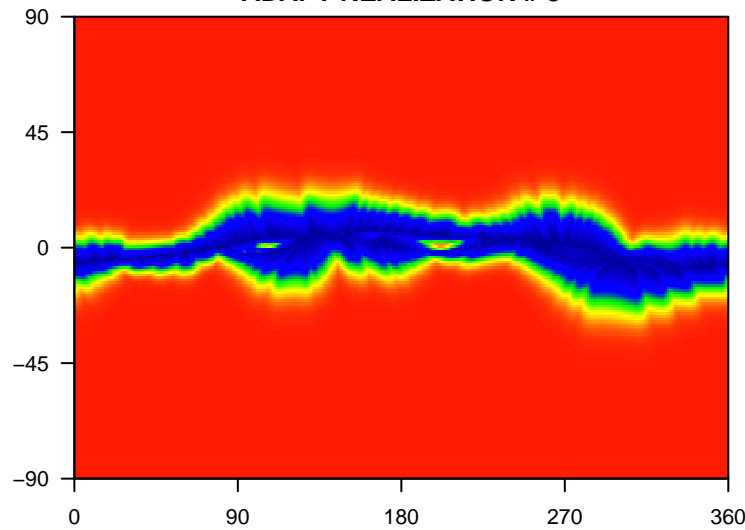
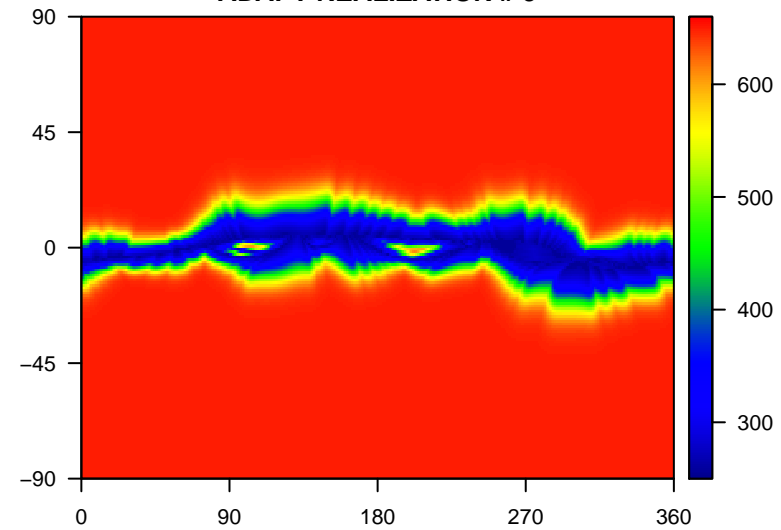
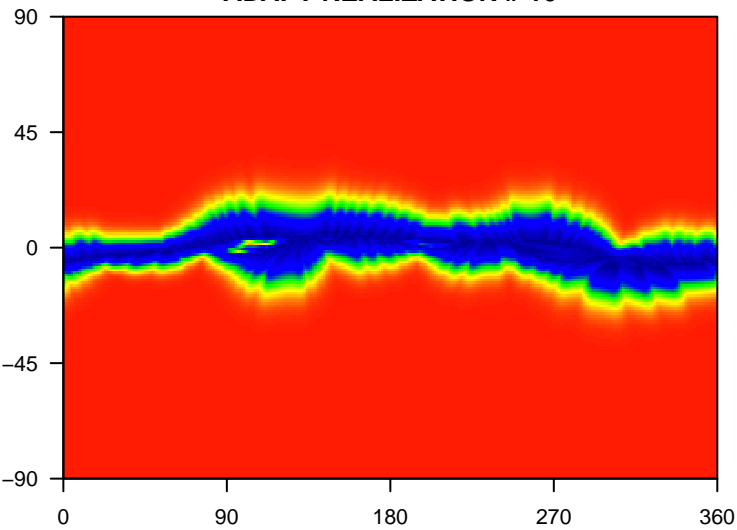
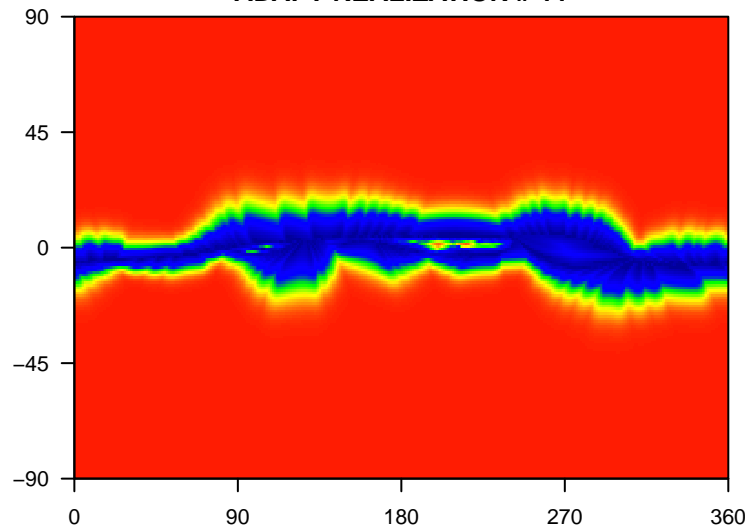
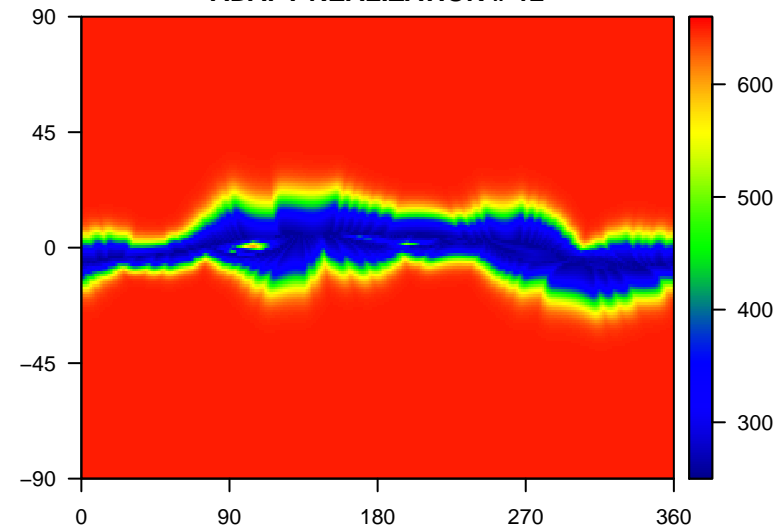
ADAPT REALIZATION # 11



ADAPT REALIZATION # 12



**Figure.**

**ADAPT REALIZATION # 1****ADAPT REALIZATION # 2****ADAPT REALIZATION # 3****ADAPT REALIZATION # 4****ADAPT REALIZATION # 5****ADAPT REALIZATION # 6****ADAPT REALIZATION # 7****ADAPT REALIZATION # 8****ADAPT REALIZATION # 9****ADAPT REALIZATION # 10****ADAPT REALIZATION # 11****ADAPT REALIZATION # 12**

**Figure.**

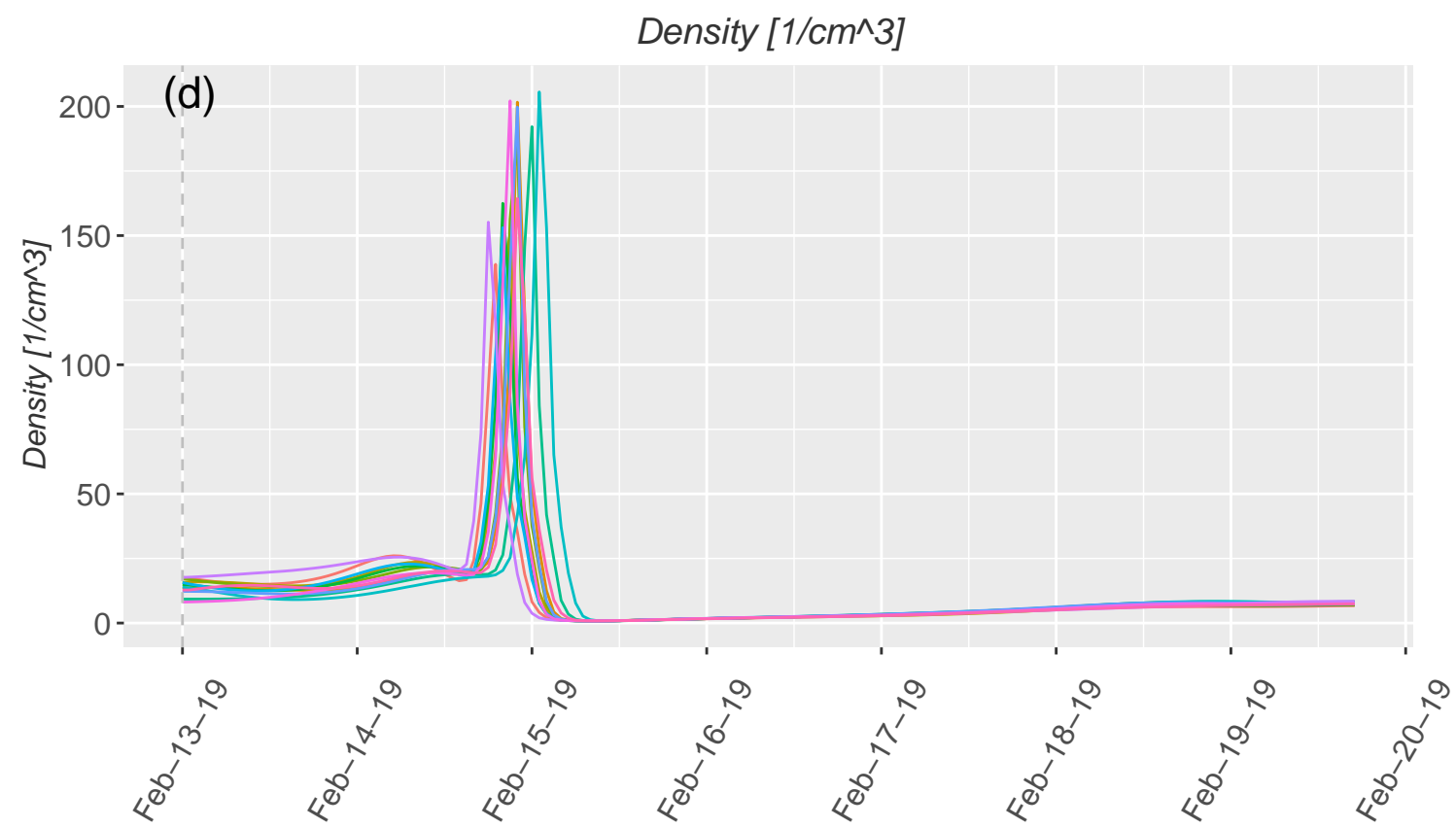
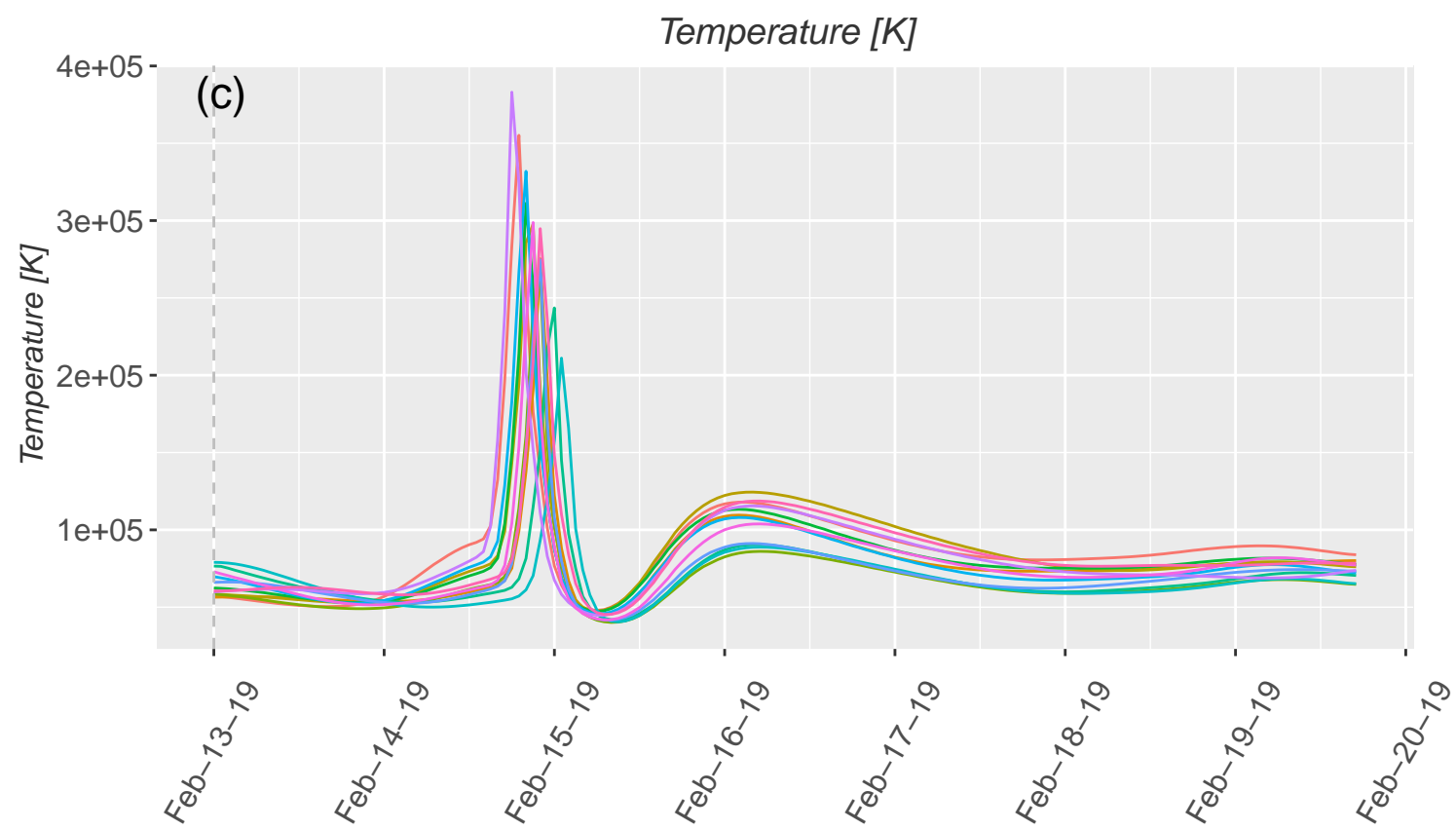
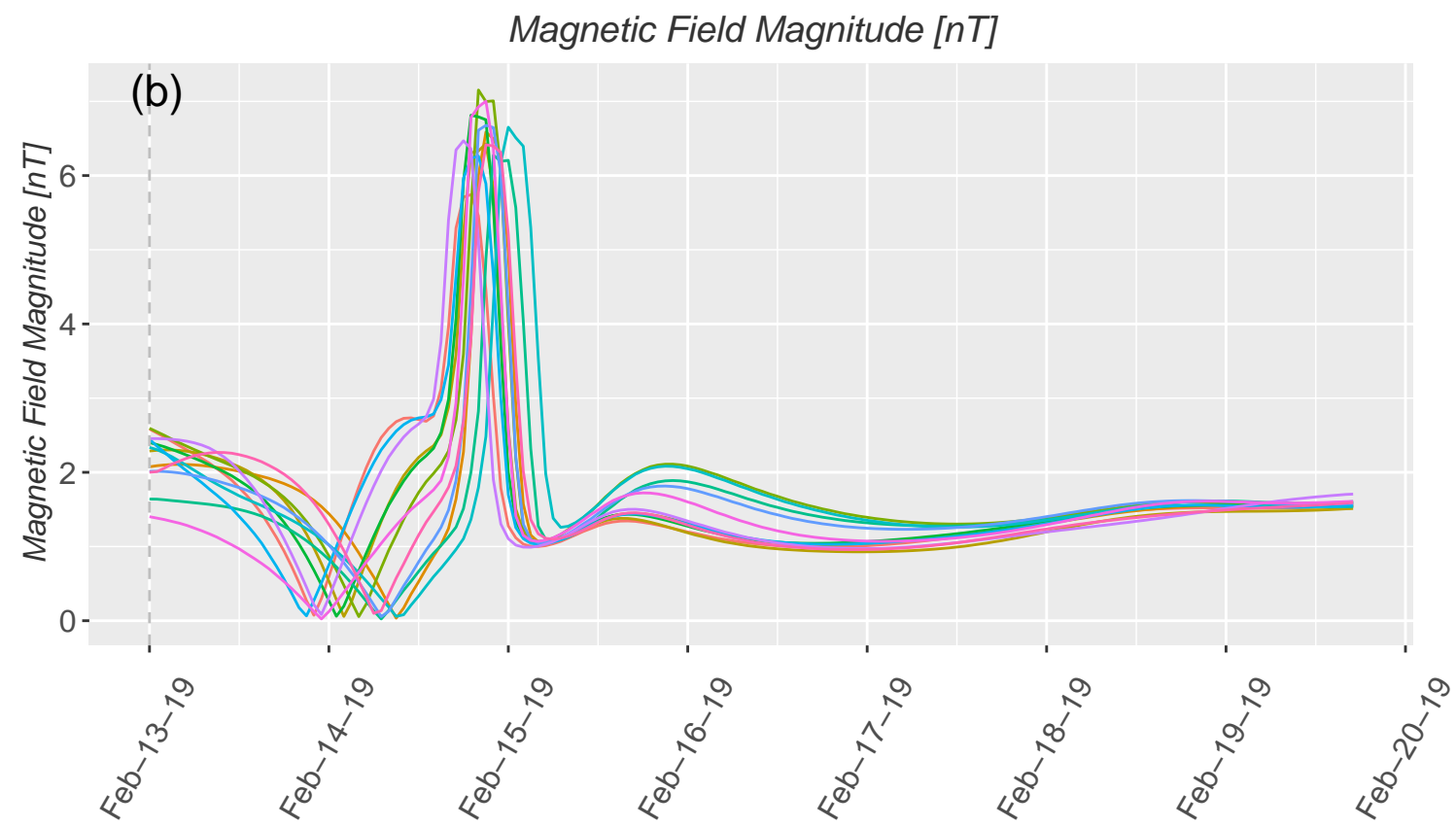
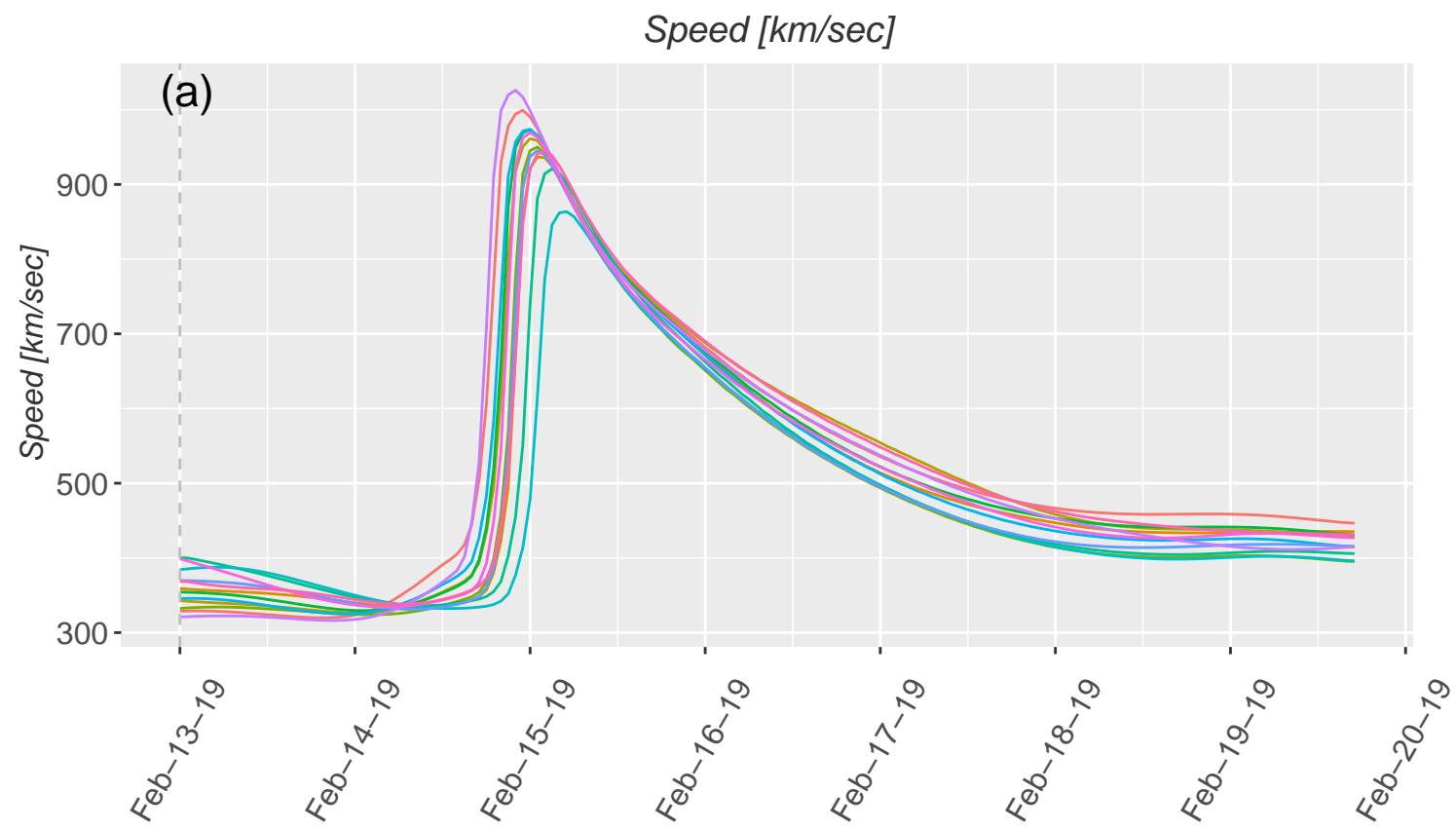


**Figure.**

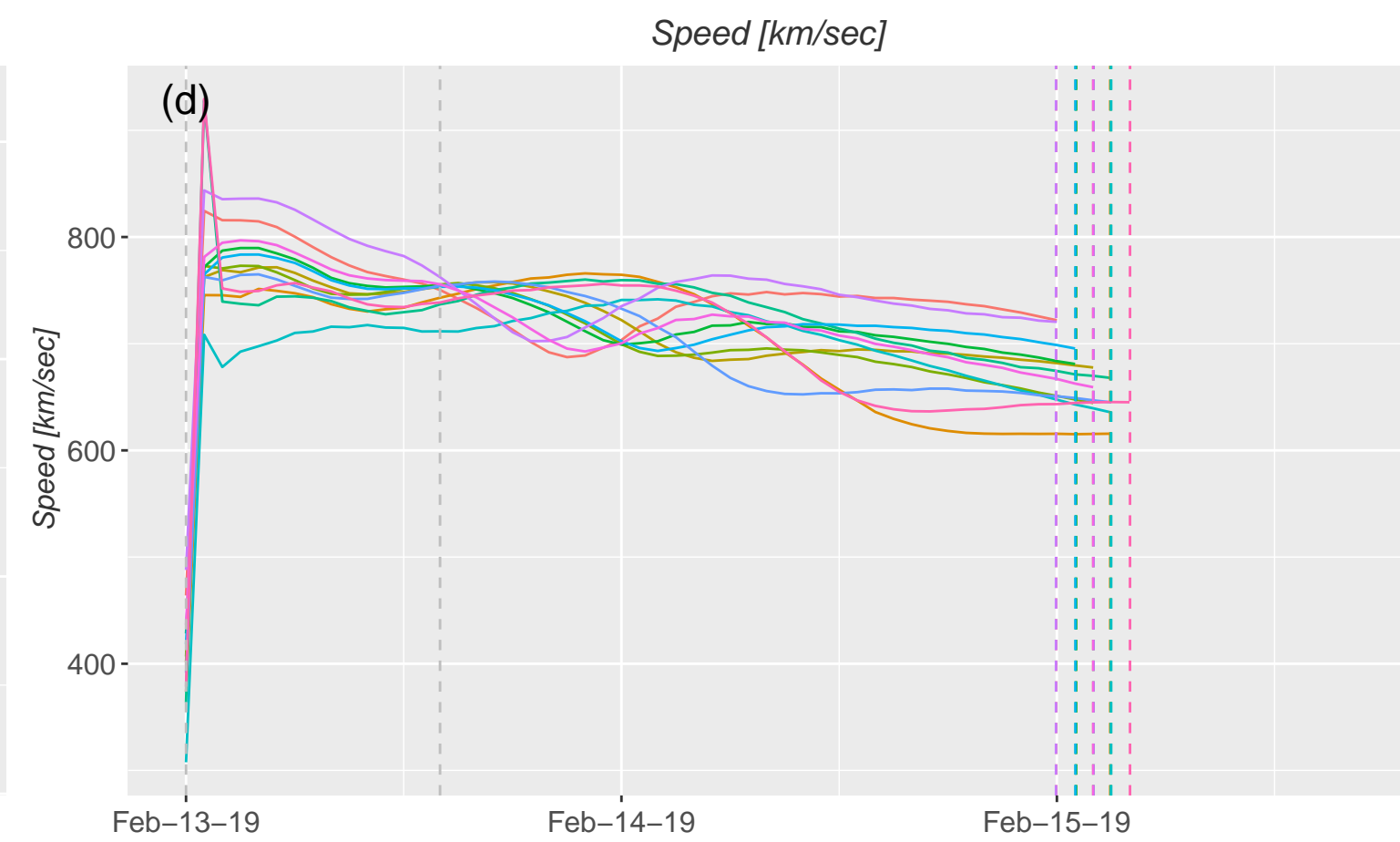
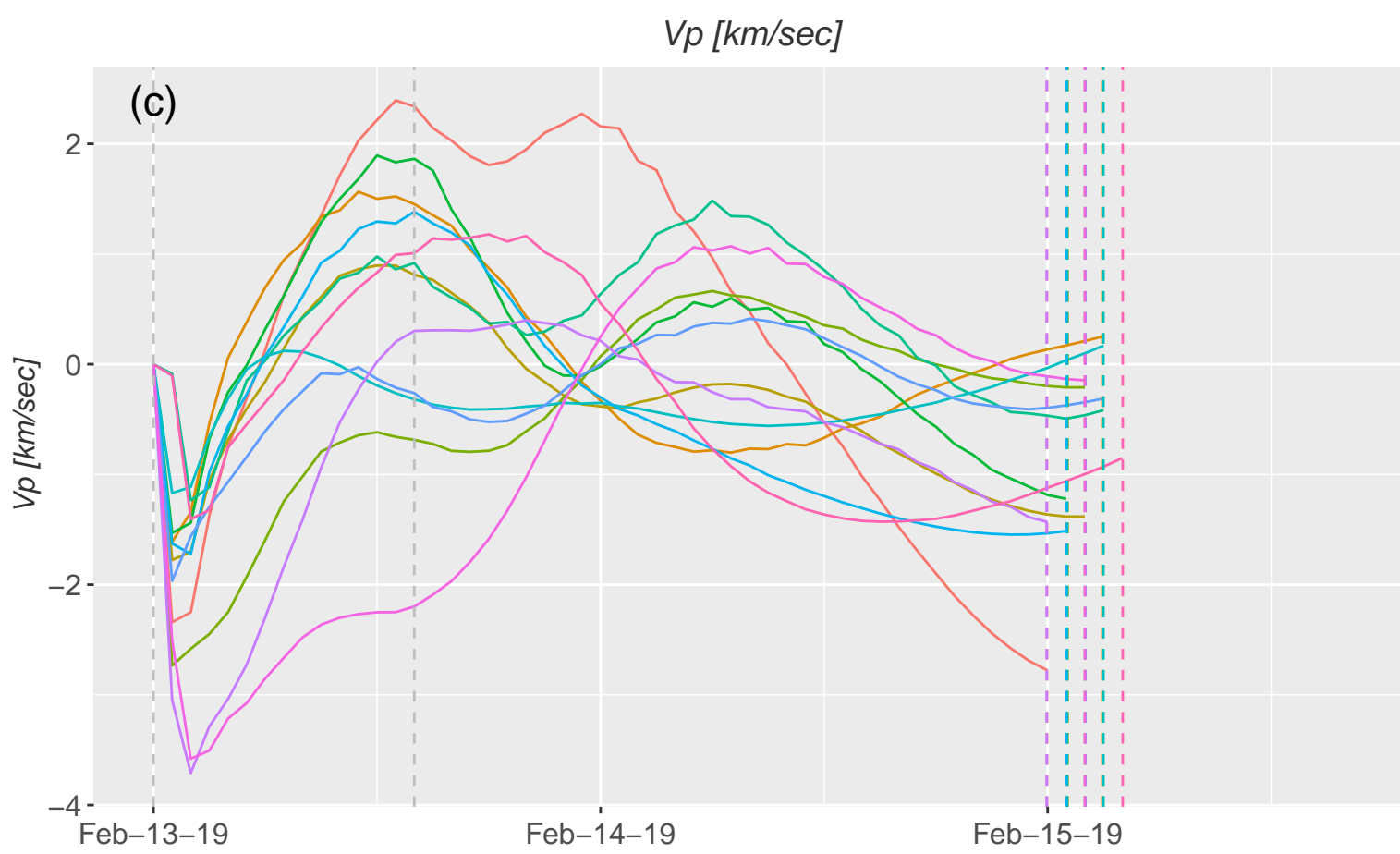
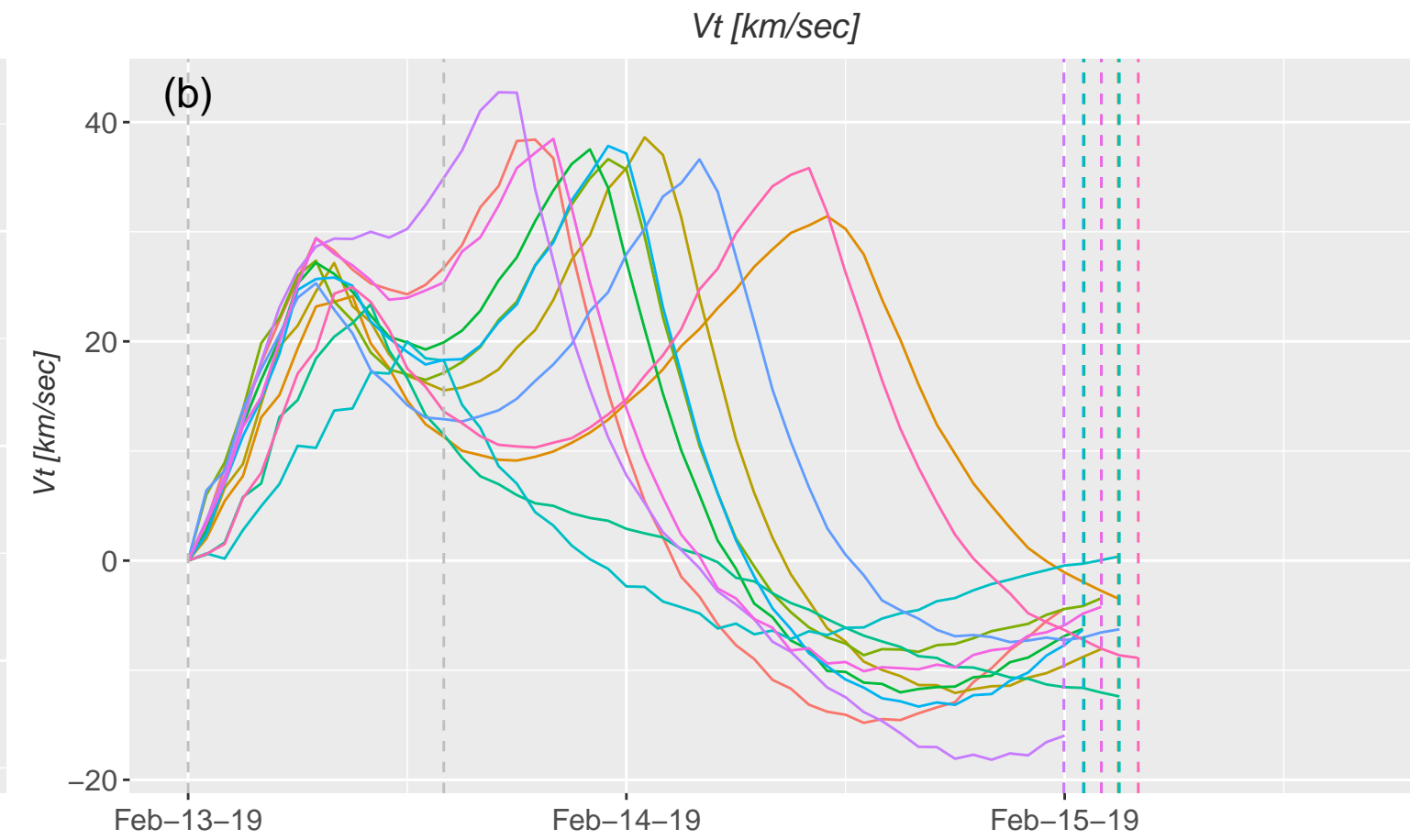
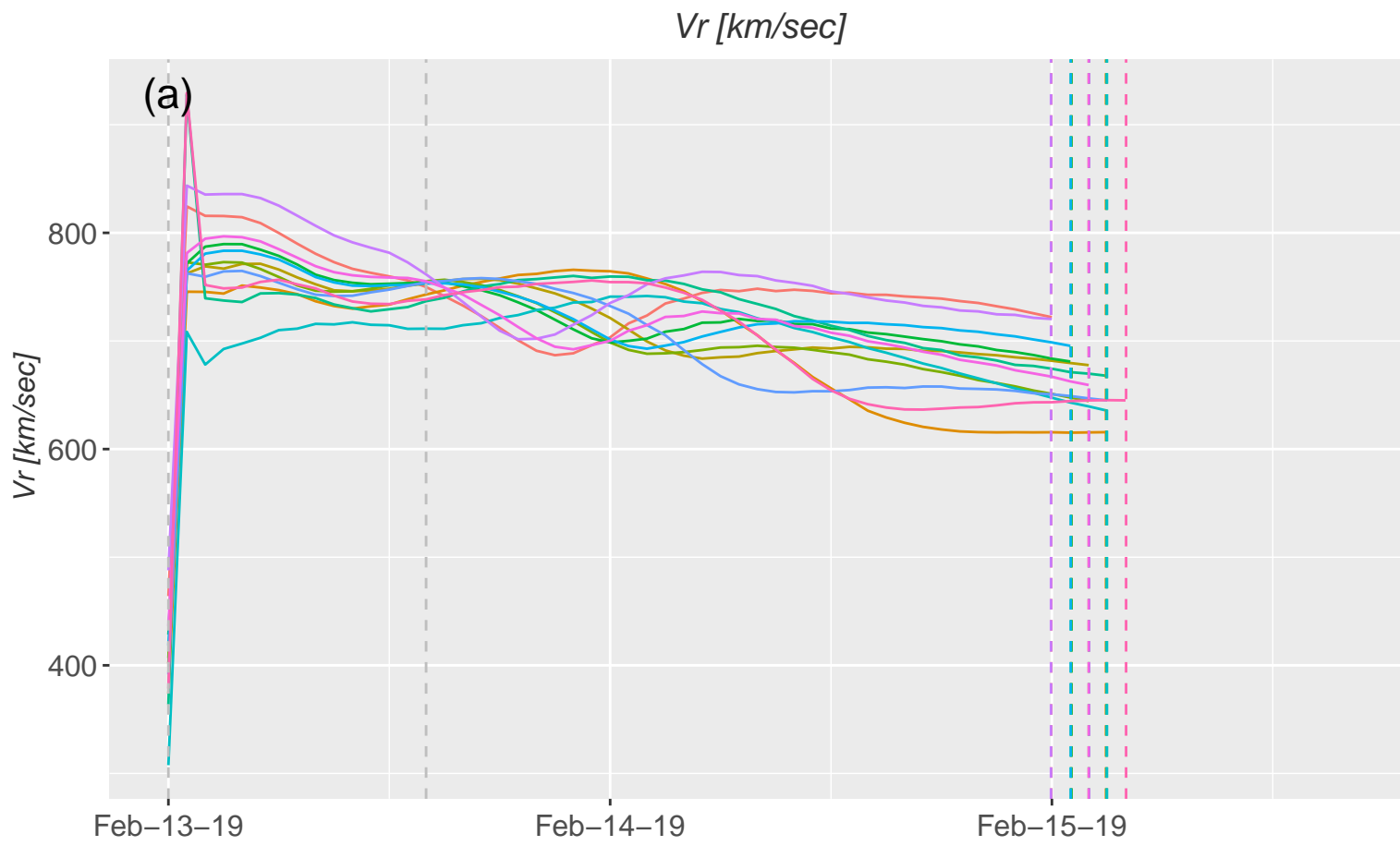


**Figure.**



**Figure.**

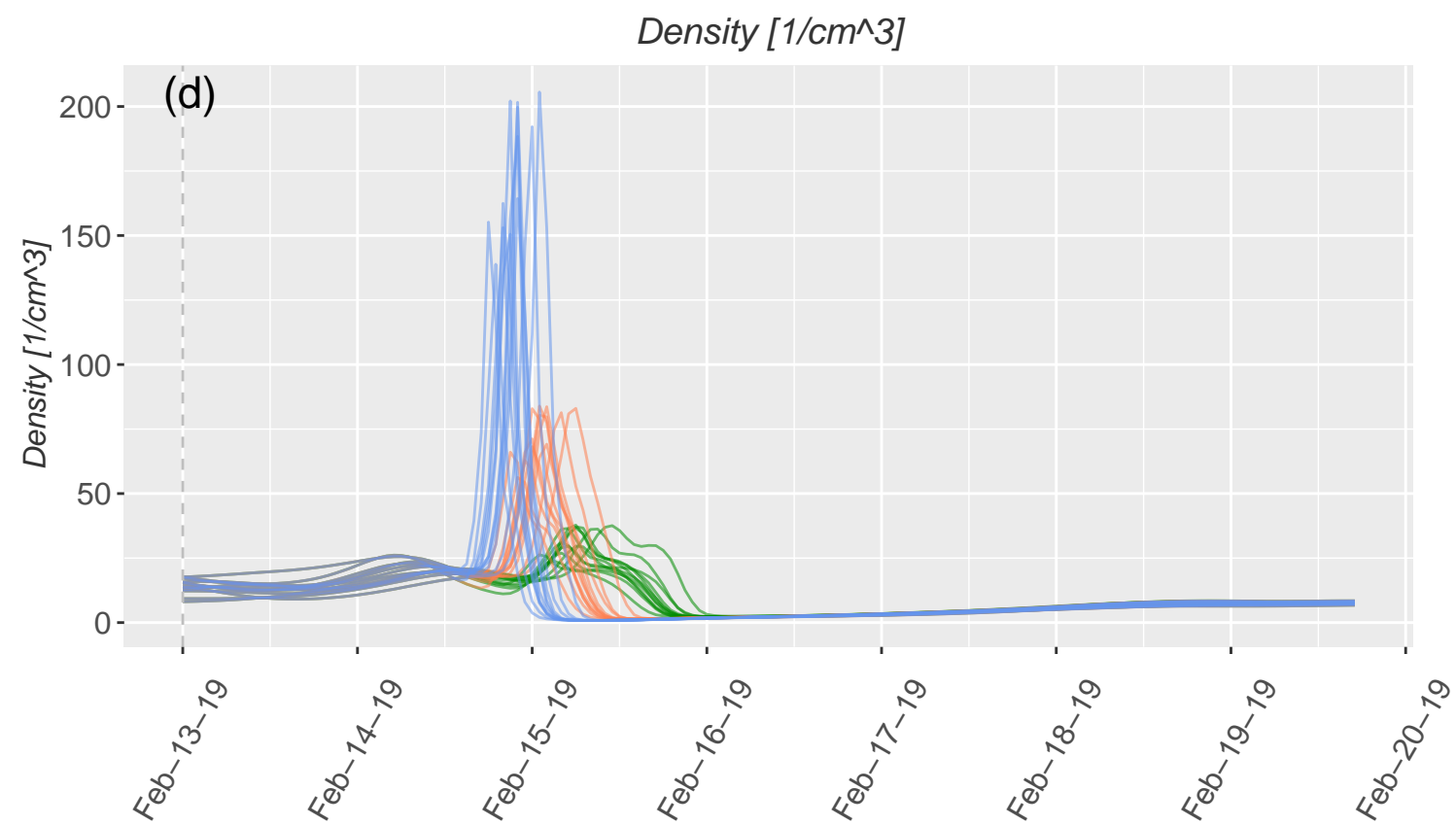
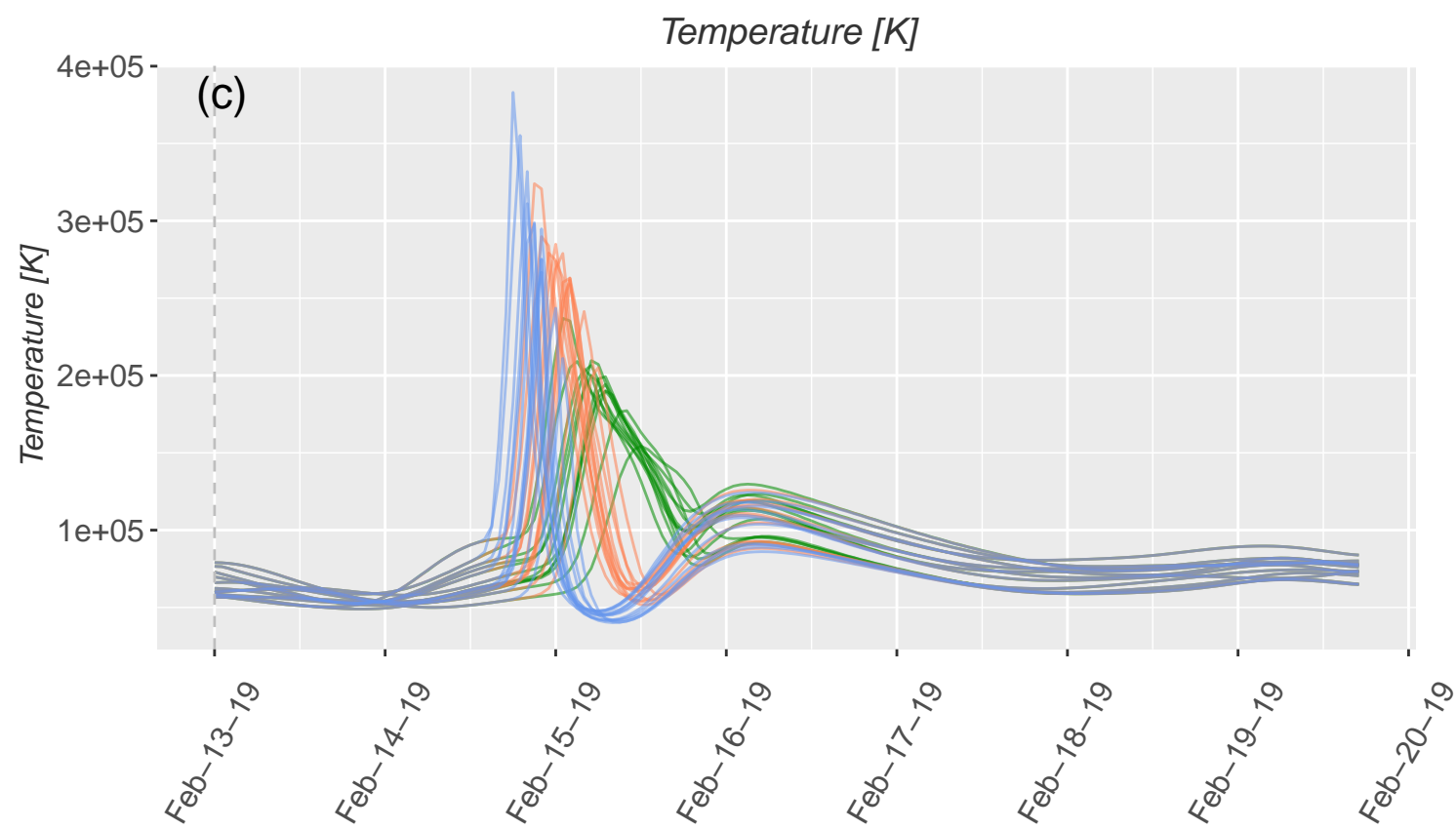
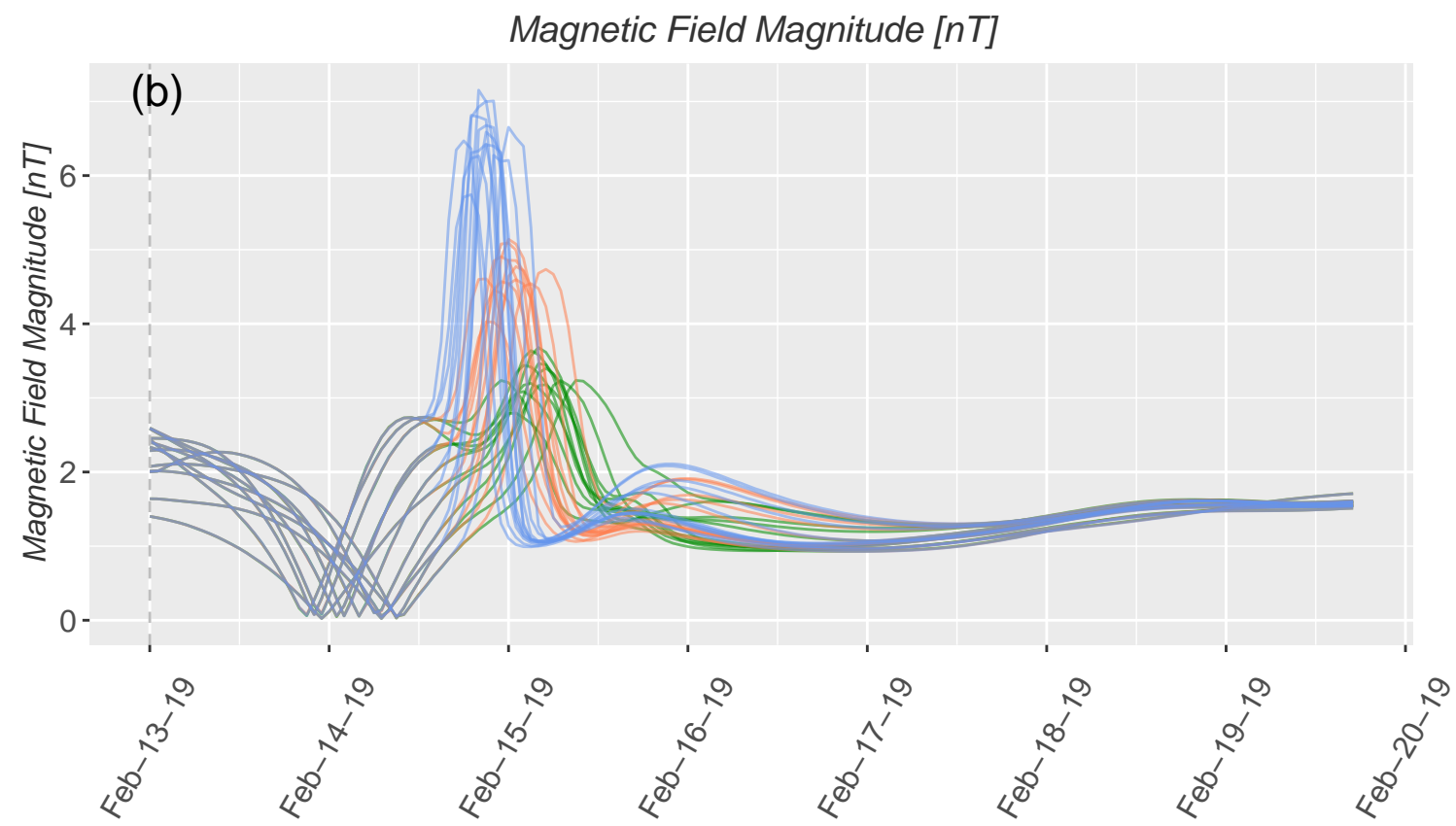
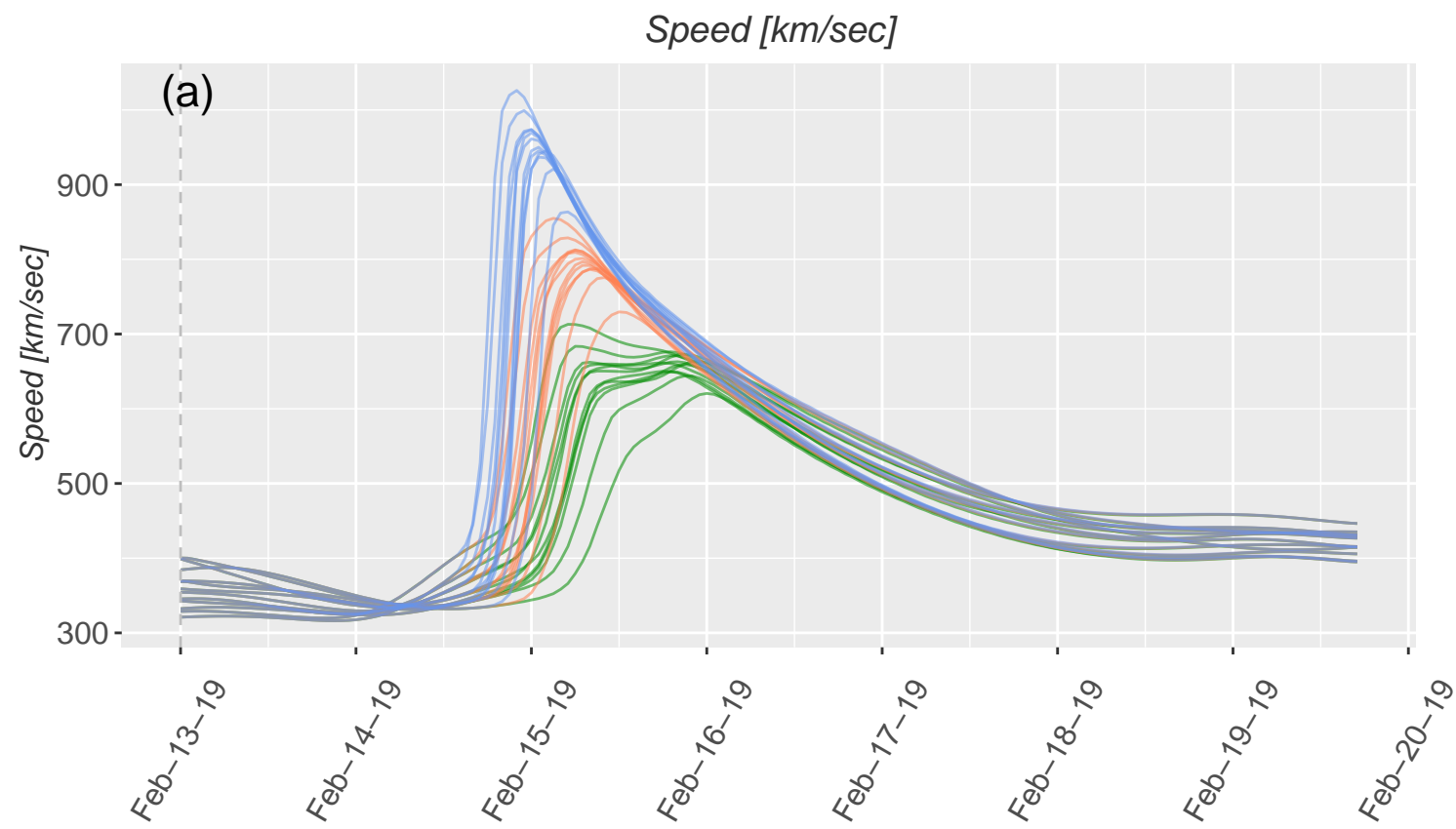


**Figure.**

